SURFACE TEXTURE DIFFERENTIATION USING SYNTHETIC BAT ECHOLOCATION CALLS: IMPLICATIONS FOR REDUCING BAT FATALITIES AT WIND TURBINES

By

BRAD YUEN

Bachelor of Arts, 2009
Boston University
Boston, Massachusetts

Submitted to the Graduate Faculty of the
College of Science and Engineering
Texas Christian University
in partial fulfillment of the requirements
for the degree of

Master of Science

December 2015

SURFACE TEXTURE DIFFERENTIATION USING SYNTHETIC BAT ECHOLOCATION CALLS: IMPLICATIONS FOR REDUCING BAT FATALITIES AT WIND TURBINES

by

Brad Rhett Yuen

Dissertation approved:

Major Professor

For The College of Science and Engineering

ACKNOWLEDGEMENTS

This thesis would not have been possible without the assistance of so many people. I would first like to thank NextEra Energy Resources for funding this research. I would also like to thank the School of Geology, Energy, and the Environment at Texas Christian University for providing me with a teaching assistantship, a stimulating learning environment, and even lodging on more than one occasion. I am particularly grateful to the three members of my thesis committee. To my advisor, Dr. Tory Bennett, thank you for painting sheet metal for me on your driveway, for guiding me, step-by-step, through the thesis-writing process, and for teaching me so much not only about bats, but also about life. To Dr. Amanda Hale, thank you for assisting me in developing the experimental design, for advising me on the presentation of my results, and not least of all, for sacrificing a room in your home to become the sound studio. To Dr. Brent Cooper, thank you for introducing me to a new world of bioacoustics analysis, for spending long hours working with me to understand these complex results, and for approaching all of our discussions with a much appreciated sense of humor.

I would especially like to thank Kaye Urbano for doing a fantastic job of teaching me to program using LabVIEW and for giving me sound technical advice throughout the project. Thank you to Chrissy Bienz for helping to set up the sound studio and, of course, painting sheet metal. Thank you to Pankaj Kumar and Dr. Bruce Miller for guiding my understanding of sound physics. Thank you also to Aaron McAlexander, Esther Chitsinde, and James Taylor for advice and support. Lastly, I would like to thank my wonderful friends and family who kept me sane over the course of this project. You made this journey worthwhile. Thank you all so very much!

TABLE OF CONTENTS

LIST OF FIGURES

LIST OF TABLES

INTRODUCTION

Wind power is a fast-growing renewable energy source with great potential to reduce pollution, water consumption, and greenhouse gas emissions (Ledec 2011, REN21 2015). Nevertheless, the large numbers of dead bats that have been discovered beneath operating wind turbines have raised concerns about its environmental sustainability (Kunz et al. 2007, Arnett et al. 2008). From 2000 to 2011, bat mortality at utility-scale wind turbines in North America was estimated to be 650,000 to 1,300,000 bats, which translates to an annual fatality rate of 54,000 to 108,000 bats per year (Arnett and Baerwald 2013). However, due to continued growth in the wind energy industry, the estimated mortality in 2012 alone was >600,000 bats (Hayes 2013, but see Huso and Dalthorp 2014). Three migratory, tree-roosting bat species (collectively known as tree bats), the hoary bat (*Lasiurus cinereus*), eastern red bat (*Lasiurus borealis*), and silver-haired bat (*Lasionycteris noctivagans*), make up 78% of total fatalities with peak fatality rates occurring between July and October, which coincides with fall migration (Kunz et al. 2007, Baerwald and Barclay 2011, Arnett and Baerwald 2013, Hein et al. 2013). Although reliable population estimates are lacking for these and other affected bat species, annual fatalities at wind turbines may have population-level consequences because bats are long-lived and have low reproductive rates which limits their ability to recover from declines (Barclay and Harder 2003, O'Shea et al. 2003, Brunet-Rossinni and Austad 2004, Podlutsky et al. 2005).

The loss of bats due to fatalities at wind turbines may also have consequences that negatively impact humans. Around the world, bats provide invaluable ecosystem services including pollination (Arias-Coyotl et al. 2006, Winfree et al. 2011), seed dispersal (Fleming and Heithaus 1981, Mello et al. 2011), and pest control (Cleveland et al. 2006, Kunz et al. 2011). In the United States, where 44 of the 47 bat species are insectivores, insect control is the primary ecosystem service provided by bats (Harvey et al. 2011, Kunz et al. 2011). The value of this ecosystem service for agriculture in the United States is estimated to be >$3.7 billion per year (Boyles et al. 2011).

At present, we have a good understanding of the proximate causes of bat fatalities at wind energy facilities (collision with rotating wind turbine blades and barotrauma; Baerwald et al. 2008, Grodsky et al. 2011, Rollins et al. 2012). Nevertheless, we still do not have a good understanding of the reasons bats come in close proximity to wind turbines. Three broad hypotheses have been proposed to this end: (1) random chance, where wind turbine kills are simply a representative sample of bat abundance and activity in an area; (2) coincidence, where some aspect of bats' ecology (e.g., migration) brings them in close proximity to wind turbines; and (3) attraction, where bats are attracted to wind turbines because wind turbines provide resources, bats perceive wind turbines to be resources, or bats are simply curious about wind turbines (Cryan and Barclay 2009). While some bat species and individual bats are likely to be at wind turbines due to random chance and coincidence, these two hypotheses alone do not appear to be able to explain the emerging patterns of bat fatalities (Kunz et al. 2007, Arnett et al. 2008, Hein et al. 2013).

If collisions of bats with wind turbine blades were random or coincidental events, then bats would be expected to show little or no interest in the wind turbines, yet bats have often been observed altering their course to fly toward wind turbines (Horn et al. 2008). Bats have also been observed investigating the blades and surfaces of stationary and rotating wind turbines, flying to offshore wind turbines, and landing on wind turbine surfaces (Horn et al. 2008, Ahlén et al. 2009, Cryan et al. 2014). Furthermore, pre-construction bat activity has been an unreliable predictor of post-construction fatalities; reports from pre-construction surveys and post-construction monitoring suggest that bat activity increases at wind energy facilities after completion (Hein et al. 2013, unpublished data). Thus, it seems likely that at least some proportion of bats come into contact with wind turbines because they are attracted to them.

Features of wind turbines hypothesized to attract bats include turbine lights, motion, sound, the modified landscape associated with wind turbines, and the potential for wind turbine structures to be

perceived as a resource (e.g., as a roost, foraging site, water source, or mating site; Cryan and Barclay 2009, McAlexander 2013). Although most of these hypotheses have not yet been sufficiently tested, some of them have been explored. To date, only the hypothesis that bats are attracted to wind turbine lights has been ruled out as fatalities were not different or were lower at wind turbines with FAA red aviation lighting compared to those without (Arnett et al. 2008, Baerwald and Barclay 2011, Bennett and Hale 2014). Horn et al. (2008) observed bats pursuing moving turbine blades, suggesting that bats are attracted to their motion. Additionally, the common wind turbine colors of 'pure white' and 'light grey' were found to attract more insects than other colors, and could represent a foraging resource to which insectivorous bats may themselves be attracted (Long et al. 2011). Finally, Cryan et al. (2014) found behavioral evidence to suggest that the airflow profile downwind of slowly rotating wind turbines is similar to those of tall trees which typically provide bats with roosting, foraging, and mating opportunities. Thus, there are many reasons why bats may be attracted to wind turbines and if we can identify these reasons, then we may be able to reduce bat fatalities.

The bat species commonly comprising fatalities at wind energy facilities all use echolocation rather than sight to navigate and capture prey (Barclay 1986, Obrist and Wenstrup 1998). By emitting ultrasonic vocalizations (>20 kHz) and listening to the returning echoes, bats are able to generate and analyze a three-dimensional representation of the world around them (Moss and Surlykke 2001). By controlling the timing, duration, and frequency of their outgoing source calls and analyzing the intensity, spectral, and temporal characteristics of the returning echoes, bats are able to negotiate complex environments, avoid obstacles, determine the range, size, shape, and texture of small moving objects, and identify water and other surfaces (Aytekin et al. 2010, Greif and Siemers 2010, Falk et al. 2011, Moss et al. 2011). Echolocation in bats is a highly sophisticated perceptual system, which is one reason why the high number of bat fatalities at wind turbines is surprising.

In 2010, Greif and Siemers discovered that bats of many species identify smooth, flat, extended surfaces (metal, wood, or plastic) to be water. Across a range of tested species, bats repeatedly attempted to drink from smooth surfaces, despite contradictory sensory information (including olfactory differences and being able to fly underneath the surfaces). However, these bats did not attempt to drink from textured surfaces. Based on this finding, Greif and Siemers (2010) proposed that bats identify water based on the acoustic properties of echoes reflecting off of its surface. Water provides a smooth surface for specular (mirror-like) acoustic reflection, in which reflected echoes travel in parallel in a single direction across the normal to the surface (Vorländer and Mommertz 2000). In contrast to smooth surfaces, textured surfaces produce scattering (diffuse reflection) which includes single and multiple reflections from surface features (Fig. 1; Pierce 1989; Vorländer and Mommertz 2000).

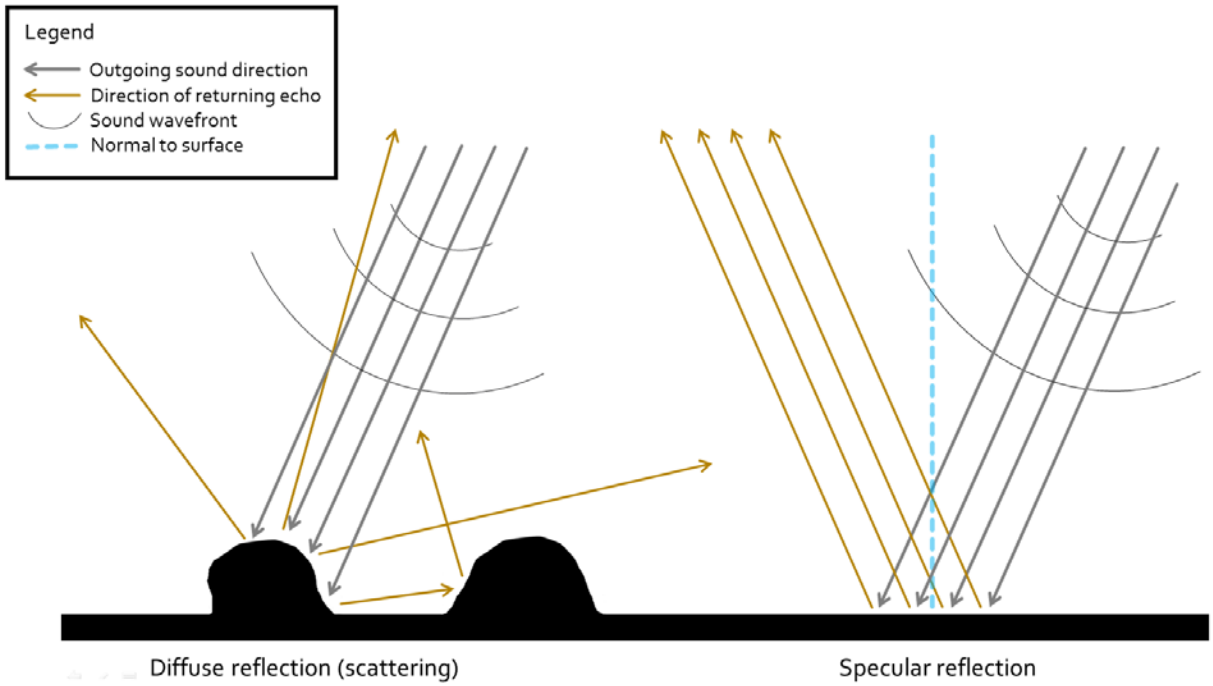

Figure 1. Simplified representation of the difference between diffuse reflection (left) and specular reflection (right). Specular reflection is characterized by reflected echo energy travelling in a single direction across the normal to the surface, whereas diffuse reflection is characterized by single and multiple reflections from surface features in multiple outgoing directions.

Greif and Siemers (2010) proposed that bats probably perceive other smooth, flat, extended anthropogenic surfaces, such as automobile hoods to be water. As many wind turbine surfaces are also smooth, flat, and extended, McAlexander (2013) proposed and tested a novel attraction hypothesis that bats may also misperceive smooth wind turbine tower surfaces to be water. In this study, an ultrasonic playback experiment within the frequency range of bat echolocation calls (20-70 kHz) revealed no discernable difference between echoes returning from wind turbine towers and water. Furthermore, bats observed using night vision displayed similar approaches and postures when drinking at water sources and when making contact with wind turbine towers (McAlexander 2013). Observations and publicly-available video of bats investigating various wind turbine surfaces in the literature are also consistent with this water-attraction hypothesis (Horn et al. 2008, Ahlén et al. 2009, Cryan et al. 2014).

McAlexander (2013) suggested that if the acoustic similarity between wind turbine towers and water contributes to bat-wind turbine collisions, then steps to reduce the similarity between wind turbine towers and water should reduce bat fatality rates at wind turbines. We hypothesized that incorporating texture additives (e.g., sand) as part of the wind turbine paint coating could alter the acoustic properties of wind turbine towers such that ultrasonic echoes returning from these modified towers could be differentiated from those returning from smooth surfaces. We further hypothesized that addition of texture additives with larger particle sizes would result in greater acoustic differences from smooth surfaces. As an initial step in testing these hypotheses, we conducted an ultrasonic playback experiment with the objective of determining the extent to which these modified surfaces could be differentiated from smooth surfaces using synthetic bat echolocation calls. In order to achieve our objective, we characterized the acoustic features of echoes returning from synthetic bat echolocation calls played at a range of smooth and textured surfaces.

METHODS

We conducted experimental trials in which we played synthetic bat echolocation calls (hereafter referred to as source calls) at experimental surfaces in a sound-dampened room. We recorded the returning echoes and acquired intensity, spectral, and temporal measurements as potential acoustic features bats may use to differentiate smooth and textured surfaces.

Angles of Incidence

We expected the acoustic characteristics of the returning echoes to vary depending upon the angle at which the calls were played at the surfaces (cf. Genzel and Wiegrebe 2008, Greif and Siemers 2010). This is relevant because bats typically echolocate at objects using a range of angles, even varying head direction, to acquire information about their three-dimensional structures (Genzel and Wiegrebe 2008, Genzel et al. 2012, Geipel et al. 2013). As bats are therefore likely to use multiple angles for echolocation, we selected three angles of incidence for our playback experiment. The angles that we chose were 0°, 20° and 40° (see Fig. 2 for a simplified representation). These angles of incidence represented a range of angles at which bats are likely to echolocate with respect to a surface. Additionally, the 0° angle of incidence replicated the playback angle used by used by McAlexander (2013) and the 40° angle of incidence replicated the angle used by Greif and Siemers (2010).

Source Calls

We created source calls across a range of frequencies representative of echolocation calls for eight North American bat species. Six of these species (hereafter referred to as local species) are known to be present in both acoustic detection surveys and fatality monitoring at a study site in North Central Texas where wind-wildlife research has been ongoing since 2009: eastern red bat (*Lasiurus borealis*; hereafter abbreviated as Labo), hoary bat (*Lasiurus cinereus*; hereafter abbreviated as Laci), silver-haired

bat (*Lasionycteris noctivagans*; hereafter abbreviated as Lano), tri-colored bat (*Perimyotis subflavus*; hereafter abbreviated as Pesu), evening bat (*Nycticeius humeralis*; hereafter abbreviated as Nyhu), and Mexican free-tailed bat (*Tadarida brasiliensis*; hereafter abbreviated as Tabr). The remaining two species are the little brown myotis (*Myotis lucifugus*; hereafter abbreviated as Mylu) and the northern long-eared myotis (*Myotis septentrionalis*; hereafter abbreviated as Myse). These latter two species are of conservation concern with ranges that overlap important wind resource areas and have both been identified in fatality monitoring at wind energy facilities (Johnson 2005, Frick et al. 2010, Langwig et al. 2012).

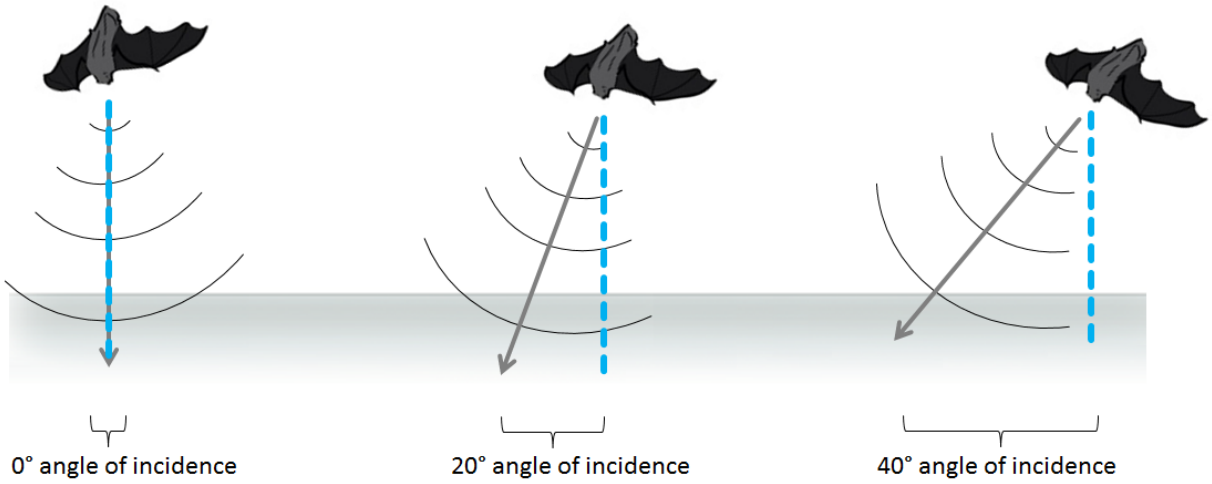

Figure 2. Illustration of angles of incidence used in the playback experiment relative to a surface. The solid grey line represents the ray of the outgoing sound direction and the dashed blue line represents the normal to the surface.

We generated 23 synthetic source calls using the dialogue synthesizer function in Avisoft Sound Analysis and Synthesis Laboratory (SASLab Pro version 5.2, Avisoft Bioacoustics, Berlin, Germany). We opted to use synthetic rather than natural calls collected from acoustic monitoring because the latter often contained high levels of background noise that would obscure our results. Furthermore, natural

calls tended to be long in duration (e.g., 6 ms for Laci calls) which meant that source calls and echoes would overlap temporally in our experiment (i.e., the source call would still be playing when the echo returned). Temporal overlap of the source call and echo makes it difficult to extract the echo from the source call, which we would need to do to effectively analyze the echo.

We created two different sets of source calls: (1) frequency-modulated (FM) sweeps, to investigate the role of frequency range on returning echoes, and (2) representative synthetic bat calls of the aforementioned 8 bat species, to investigate different acoustic characteristics that a variety of bat species might use to differentiate smooth and textured surfaces. To keep intensity constant between source calls, all calls were generated by setting the maximum amplitude to 500 mV and setting the amplitude fading to a sine 1/2 shape in order to create a smooth inverted U-shaped amplitude profile. To create source calls with high temporal resolution without substantial loss of frequency resolution, we digitized the calls at a 500 kHz sampling rate. Source calls were subsequently saved into a playlist in WAV file format (.wav) with 100-150 ms silent intervals between the calls to ensure that we did not record room reverberations (i.e., multiple temporally-overlapping echoes returning from the surfaces of the room; Appendix A).

Synthetic FM Sweeps

To compare our results with those of Greif and Siemers (2010), we replicated their source call which was a 3 ms, linear FM sweep from 120 to 20 kHz encompassing the echolocation frequency range of European bats (Fig. 3, call 1). Additionally, we created eight linear 1.5 ms, FM sweeps of 10 kHz bandwidth beginning at 30-20 kHz and ending at 100-90 kHz (Fig. 2, calls 2-9) to encompass the echolocation frequency range of North American bats.

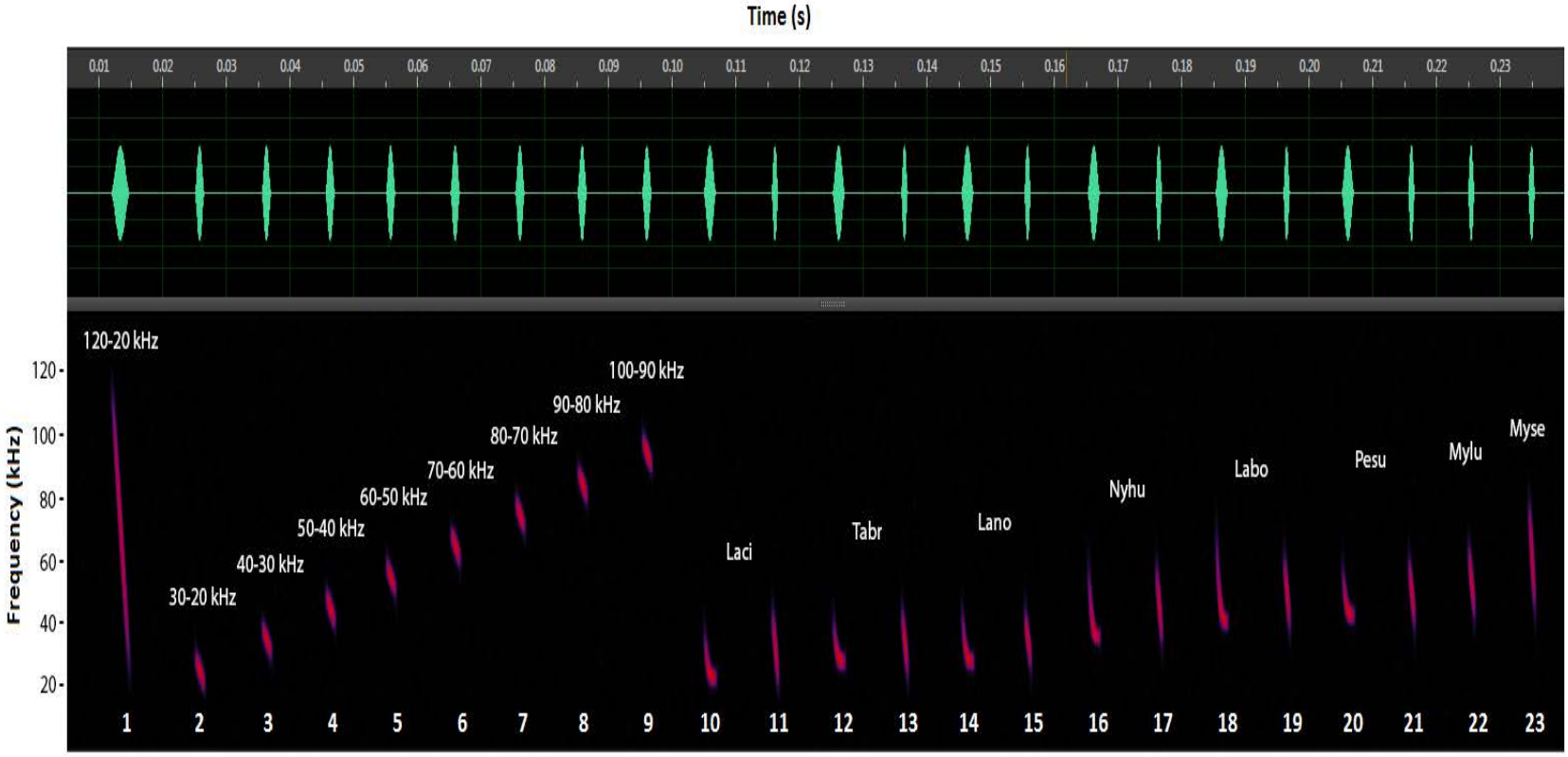

Figure 3. Oscillograms (top panel) and spectrograms (bottom panel) of source calls used in the playback experiment as viewed in Adobe Audition CS6 (Version 5.0.2; Adobe Systems Inc., San Jose, CA) sound editing software. Calls 1-9 are synthetic FM sweeps. Calls 10-21 are synthetic approach and terminal buzz calls representative of the 6 bat local bat species. Calls 22-23 are synthetic terminal buzz calls based on frequency measurements of Mylu and Myse calls, respectively (See Appendix A for list of calls).

Synthetic Bat Calls

When bats echolocate, they vary their call structure depending on proximity to their target of interest (Griffin et al. 1960, Surlykke and Moss 2000). To uncover the effect that these different call structures have on texture differentiation, we created 14 source calls in two categories after Griffin et al. (1960): (1) approach calls, which are emitted by bats after they have located an object of interest and are closing in on it, and (2) terminal buzz calls, which are emitted by bats just prior to an attempted prey capture, landing, or drinking event (Melcón et al 2009; Griffiths 2013; Ratcliffe et al. 2013; see Fig. 4). Of these 14 synthetic bat calls, six were approach calls (one for each local species) and eight were terminal buzz calls, (one for each local species and one each for Mylu and Myse). We generated these short-duration, synthetic bat calls based on mean high- and low-frequency measurements (n = 20 to 30 natural calls each) obtained from full spectrum recordings of actual bats for each of the six species at the local study site and generated Mylu and Myse terminal buzz calls based on zero-crossing recordings obtained in the Upper Penninsula of Michigan. We did not generate synthetic approach calls for Mylu and Myse because the low resolution of the zero-crossing recordings did not permit reliable reproduction of the entire call. Note that the 2 ms approach calls appear slightly curved on a spectrogram which is typical of natural approach calls (Griffin et al. 1960; Fig. 3, calls 10, 12, 14, 16, 18, and 20), while the 1 ms terminal buzz calls were linear, representative of actual terminal buzz calls (Fig. 3, calls 11, 13, 15, 17, 19, 21, 22, and 23).

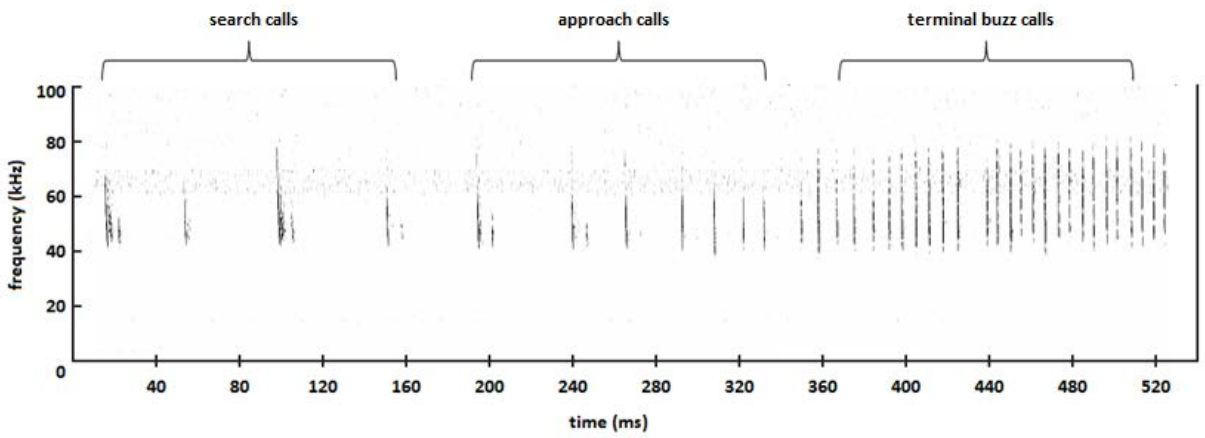

Figure 4. Example sonogram (Labo) showing the distinction between approach and terminal buzz calls. Search calls are included in this sonogram but were not used in the playback experiment.

Experimental Surfaces

We created six surfaces from galvanized steel sheets (1 m x 1 m): smooth unpainted metal which is equivalent to a surface bats perceive to be water (Greif and Siemers 2010), smooth painted metal which represents current wind turbine tower surfaces, three textured, painted wind turbine tower alternatives with varying texture particle sizes, and a wood chip surface which represents a potential wind turbine texture that might be misperceived by bats to be a tree (Fig. 5). To replicate smooth, painted wind turbine tower surfaces, we used the same paint as that applied to General Electric 1.5-megawatt wind turbines. We applied two layers of Intergard 345 epoxy to one of the sheets which was subsequently painted with two layers of Interthane® 990 acrylic finish (International Paint, LLC, Houston, TX). To create textured surfaces, we applied the same paint layers to the remaining four sheets, with the inclusion of the following texture additives (2 cups per ½ gal) in the second layer of the epoxy: fine-grained sand (U.S. Mesh 20/30 or ca. 590-840 µm), medium-grained sand (U.S. Mesh 16/20 or ca. 840-1190 µm), coarse-grained sand (U.S. Mesh 10/14 or ca. 1410-2000 µm), and small wood chips.

Figure 5. Photographs of experimental surfaces (US quarter-dollar coins for scale) illustrating the range of texture treatments used in the playback experiment.

Sound Studio and Playback

We conducted the ultrasonic playback experiment in a sound-dampened room, hereafter referred to as the sound studio (dimensions 3.5 m x 3.5 m x 2.5 m; Fig. 6A). We minimized external noise by lining all four walls with household comforters and reduced the strength of reverberations within the sound studio by overlaying the comforters with polyurethane bedding foam. We installed nine additional acoustic foam panels (1.2 m x 0.6 m x 0.02 m) in strategic places to absorb secondary sound reflections. Three of these panels were placed in the corner directly behind the playback setup, two were centered on the ceiling directly above the playback setup (Fig. 6B), and the remaining four were placed on the center of the carpeted floor surrounding the experimental surfaces to absorb acoustic reflections caused by the edges of the metal plates, as actual wind turbine tower surfaces do not have

edges (Fig. 6C). Lastly, we placed two cotton batting mats (1.2 m x 0.6 m x 0.04 m) in the center of the floor between the 4 acoustic foam panels with a 1 m x 1 m masking tape square outlining the position of the different surfaces so that they could be repeatedly placed in the same location relative to the playback setup.

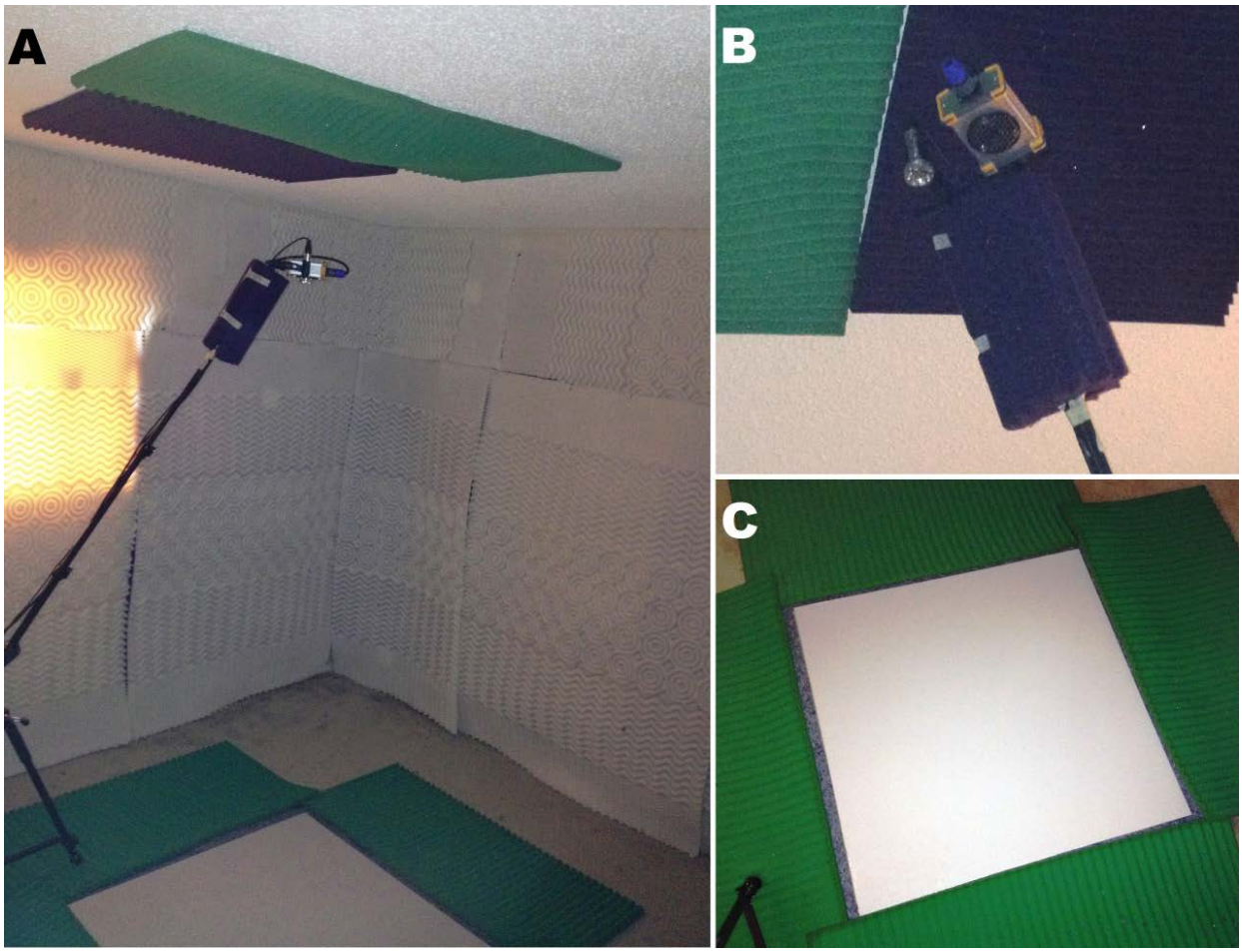

Figure 6. Views of playback equipment in the sound studio. (A) View of the sound proofing and echo dampening materials and the position of the surfaces within the room. (B) Upward view of the playback setup with ultrasonic dynamic speaker Vifa (right) and ultrasound microphone CM16/CMPA (left) mounted in parallel, 10 cm apart. (C) Aerial view of the painted surface lying flat atop two cotton batting mats and surrounded by four acoustic foam panels.

The playback setup consisted of an Avisoft Bioacoustics UltraSoundGate Player 116 (frequency range 1 - 180 kHz), recorder 116H (frequency range 20 - 460 kHz), ultrasonic dynamic speaker Vifa (± 9 dB, 20 - 100 kHz), and condenser ultrasound microphone CM16/CMPA (± 6 dB, 20 - 100 kHz). We positioned the speaker and microphone 10 cm apart on a Sabra-Som ST2 stereo bar attached to the boom arm of an AiRR 200 microphone stand (Fig. 7A). We chose a 10 cm separation distance between speaker and microphone and added a triple-thick piece of acoustic foam with multiple layers of plastic embedded in it (15 cm x 15 cm x 8 cm) between the speaker and microphone to reduce direct transmission of sound (Fig. 7). This playback setup was centered in the sound studio (Fig. 7B). To ensure that the echoes we analyzed were reflected from the experimental surfaces and not from elsewhere in the sound studio, we positioned the playback setup 0.5 m away from each surface.

Digital settings selected in the software Avisoft-RECORDER USGH (version 4.2, Avisoft Bioacoustics) were 0.5 s pre-trigger with a 2.0 s hold-time, 16-bit format, and a pre-recording buffer of 0.032 s. We performed all playback and recording at a sampling rate of 500 kHz to provide a high level of temporal resolution and to increase the robustness of the built-in anti-aliasing filter that prevents artifacts caused by undersampling. Sound recordings were saved onto a laptop computer in WAV file format for analysis.

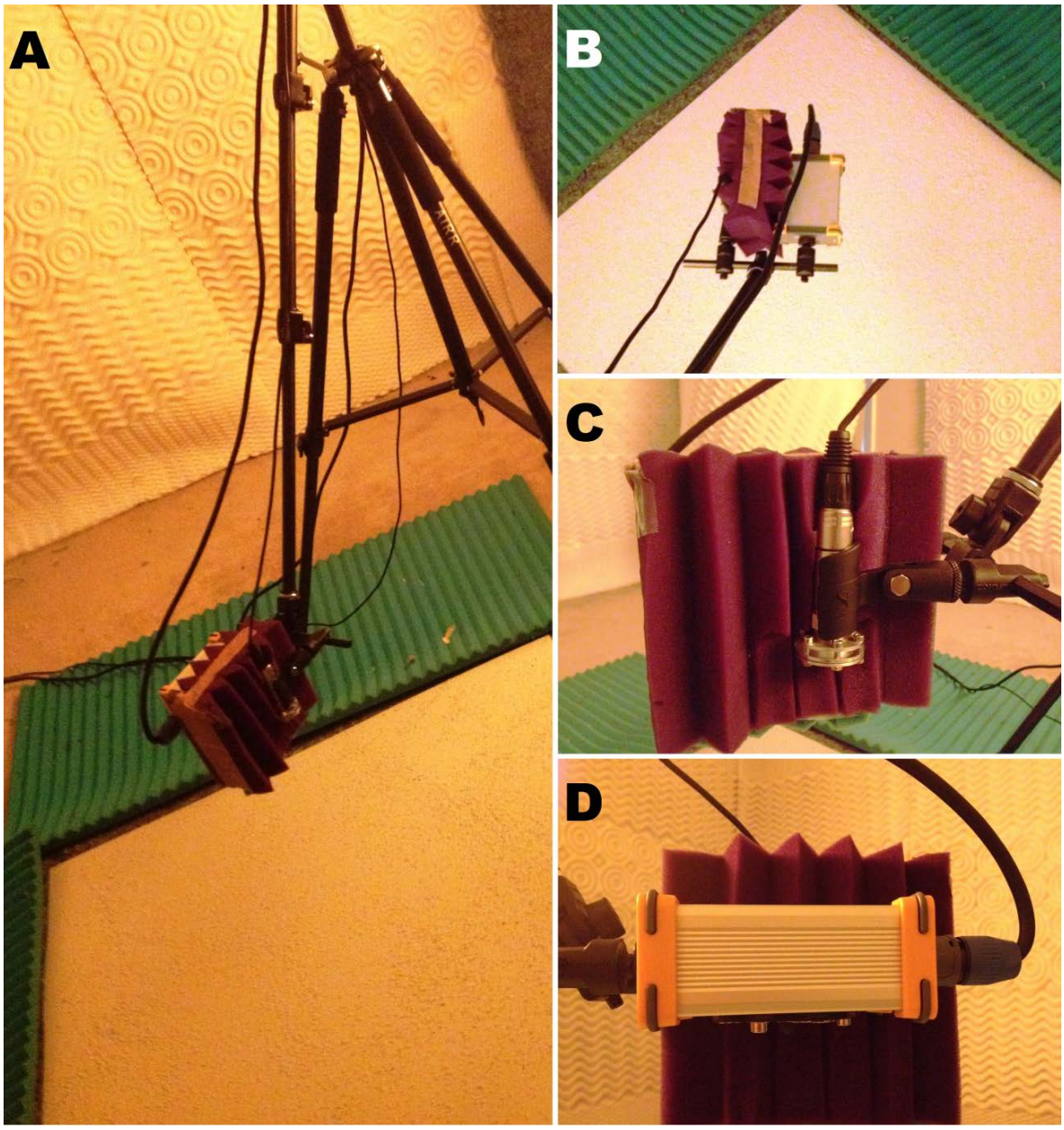

Figure 7. Views of playback setup in the sound studio (50 cm from plate to setup). (A) Side view of playback setup facing the surface at a 0° angle centered above the coarse textured plate. (B) Aerial view of the playback setup with ultrasonic dynamic speaker Vifa (right) and ultrasound microphone CM16/CMPA (left but blocked from view); layered foam and plastic positioned between the speaker and microphone. (C) Side view of the ultrasound microphone CM16/CMPA. (D) Side view of the ultrasonic dynamic speaker Vifa.

Experimental Procedure

We conducted the playback experiment on three consecutive days (September 24, 25, and 26, 2014) with each day representing a replicate to account for potential variation in the playback setup (e.g., small differences in the placement of experimental surfaces and the playback equipment) and environmental conditions (e.g., relative humidity and temperature) within the sound studio. On each day, we performed 108 experimental trials (36 trials per angle). Note that within each trial, playback was performed under fixed conditions (i.e., neither angle nor surface was changed). Due to our sampling design, which is discussed later, we divided the 36 trials for each angle into 6 sets of 6 trials each. Surfaces were switched between each trial and angle was switched after 6 sets.

Before conducting each trial, we positioned the playback setup over the appropriate experimental surface (0.5 m horizontally from each side for 0° angle trials and 0.35 m horizontally from each side and facing the center in both the 20° and 40° angle trials) so that the acoustic axis of the speaker and microphone intercepted the surface at the desired angle (0°, 20°, or 40°). The order of the three angles was randomized on each day (see Appendix B for order).

In each trial, we played the playlist containing all source calls five times (resulting in 5 repeated measurements). To control for any systematic differences not attributable to the surfaces (e.g., room temperature and humidity based on time of day), we randomized the order of all trials using a Latin square sampling design consisting of three 6 x 6 ordered matrices (Kirk 2010; an example matrix appears in Appendix C), and reset the temperature of the sound studio down to 21.5 °C after each set. This temperature was chosen because the microphone frequency response was optimized for temperatures between 20 and 25 °C (R. Specht, pers. comm.). Throughout all 6 sets for each angle on each day, the playback setup remained stationary and only the experimental surfaces were moved.

To confirm the identity of the target echo and for analysis (below), we recorded a single WAV file in each trial using a custom-built Y-Jack (courtesy R. Specht, Avisoft Bioacoustics) that allowed

simultaneous recording and projecting of calls with high temporal acuity. A time delay of ca. 2.9 ms (based on the speed of sound at 21.5-23.5 °C and a round-trip distance traveled of 1 m) between the source call and the returning echo allowed us to identify the first returning echo as the target echo. Furthermore, recording of the outgoing source call allowed us to align echoes to compare them temporally.

Finally, before the first trial and after the last trial in each day of recording, we played a 40 kHz reference sound (Avisoft Bioacoustics) with a known sound pressure level (74 dB SPL at 25 cm) 25 cm away from the microphone and recorded the sound for one minute. The purpose of this recording was to calibrate the SASLab software to convert amplitudes from full scale to decibel sound pressure level (dB SPL) for analysis.

Analysis of Recorded Echoes

All recordings were first digitally filtered with a high-pass finite impulse response filter in SASLab (17 kHz cutoff) to remove low frequency background noise. Spectrograms and amplitude envelope curves were then generated in SASLab for each recording (excluding recordings using the Y-jack; Fig. 8; see Table 1 for settings). Using these spectrograms and envelope curves, we manually selected amplitude thresholds to define the beginnings and ends of echoes. The criteria for these user-defined amplitude thresholds were that they included the full detectable echo without including direct acoustic transmission between speaker and microphone or secondary echoes reflecting off of the playback setup. To ensure consistency, a single amplitude threshold value was used for each angle-call combination (see Appendix D for threshold values). To compare the overall intensity of returning echoes, we measured the maximum peak amplitude (dB SPL) for each recording in SASLab (Fig. 8).

Table 1. Settings and resolutions for spectrograms used to measure maximum peak amplitude and mean Wiener entropy in SASLab.

Control	Setting/Resolution
FFT length	1024 point
Window type	Flat top
Frame size	100%
Bandwidth	1836 Hz
Frequency resolution	488 Hz
Temporal resolution	0.032 ms

As bats use spectral and temporal cues to distinguish echolocation targets (reviewed in Goerlitz et al. 2008), we compared spectral characteristics of returning echoes by measuring mean Wiener entropy (a measure of spectral flatness, where 0 corresponds to a pure tone with all energy at a single frequency and 1 corresponds to white noise with equal energy at all frequencies) for each recording in SASLab. To quantify differences in temporal modulation between echoes recorded from each surface, we calculated temporal waveform variation using custom tools written in LabVIEW 7.1 (National Instruments, Austin, TX). For this measurement, we only used echoes recorded using the Y-jack to take advantage of the time reference provided by recording of the source call.

To measure temporal waveform variation of each echo, we extracted 3.0 ms of sound (1500 samples at 500 kHz) beginning 2.4 ms after the start of the source signal. These sound segments included 0.5 ms of sound before the onset of the target echo and ended 0.4 ms before the earliest returning secondary echoes. We then full wave rectified these 3.0 ms extracted echoes (this is a process in which all negative amplitude values in the echo are transformed into positive values). Next, we smoothed the resulting waveforms using a 0.1 ms sliding averaging window to remove small sample-to-sample fluctuations and discontinuities in the waveforms. To minimize the effect that amplitude

differences had on the resulting measurements, we normalized the echoes by setting the highest amplitude in each echo to 1 and the lowest amplitude in each echo to 0. The rectified waveforms (hereafter referred to as transformed echoes) were used to calculate temporal waveform variation between surfaces. The transformed echo from the smooth painted surface in each set was the baseline waveform to which we compared the transformed echo from each other experimental surface in the same set. This resulted in 5 pairs of temporally-aligned transformed echoes. We calculated the sum of squared deviations between the 1500 data points of the digitized sound file for each pair of transformed echoes (painted-unpainted smooth, painted-fine texture, painted-medium texture, painted-coarse texture, and painted-wood chip; see Fig. 9 for an example).

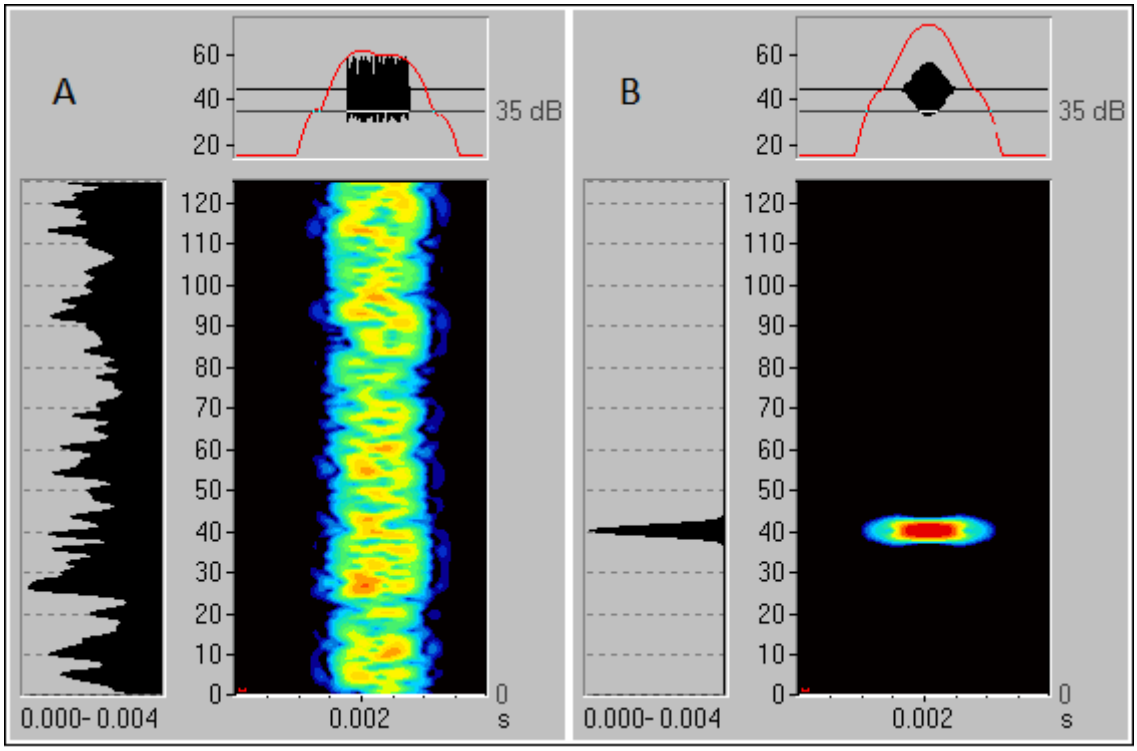

Figure 8. Echo measurements taken in SASLab. Displayed are representative spectrograms (colored images in center panels), oscillograms (black lines in top panels), amplitude envelope curves (red lines in top panels), and mean frequency spectra (left panels). (A) is white noise and (B) is a pure tone. Maximum peak amplitude is indicated by the highest value on the amplitude envelope curve (61.61 dB SPL in A and 73.08 in B). Mean Wiener entropy is calculated from the flatness of the frequency spectra (0.901 in A and 0.210 in B). The dashed purple line indicates the echo above the specified threshold (35 dB SPL).

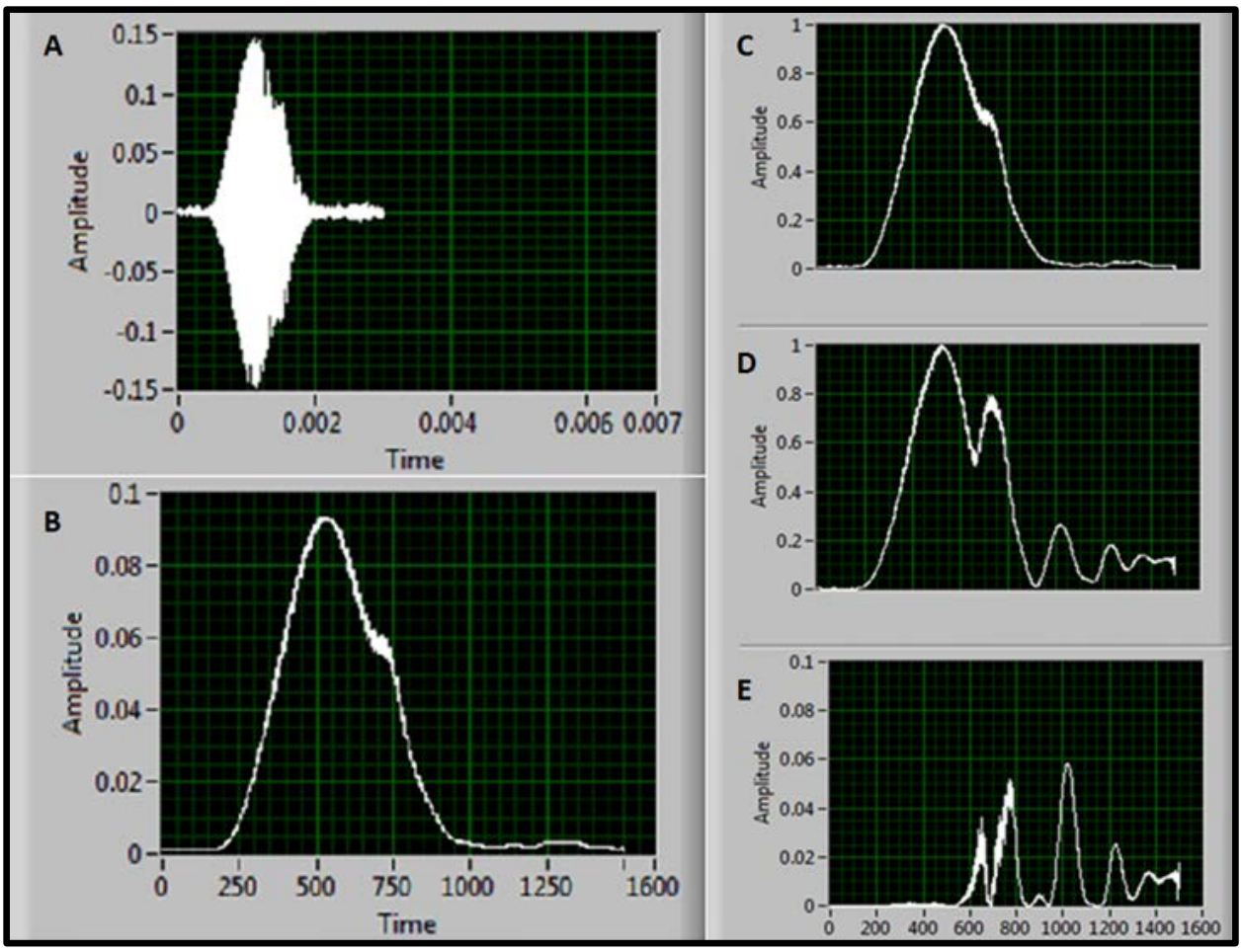

Figure 9. Representative steps in the temporal waveform variation measurement process. (A) Oscillogram of the smooth painted echo is extracted. (B) The echo oscillogram is converted into a rectified, smoothed waveform. The rectified, smoothed waveform is normalized (C) and then is subtracted from the waveform from each other surface on a sample-by-sample basis. (D) is an example of a coarse texture echo waveform. The differences between each sample in the waveforms are squared (E) and then summed, resulting in a single value per comparison (range 0-1500).

As transformed echoes from the same surface varied slightly between trials, we also calculated values for temporal waveform variation of the smooth painted surface using consecutive trials (i.e., trial 1-2, 2-3, 3-4, 4-5, and 5-6). The resulting temporal waveform variation measurements for the painted-painted comparison were essentially a measurement error, and a value below which temporal waveform variation measurements would be considered to be caused by chance, rather than reflecting a difference in temporal modulation of echoes between surfaces. To summarize the magnitude of

temporal differences between each surface and the smooth painted surface, we further calculated normalized temporal waveform variation in which we divided the temporal waveform variation for each surface comparison (i.e., painted-unpainted, painted-fine, painted-medium, painted-coarse, and painted-wood chip) by the painted-painted temporal waveform variation at each angle-call combination.

Statistical Analysis of Recorded Echoes

Since we had only a single example of each experimental surface that we tested, our trials were technically pseudoreplicates and thus failed to meet the basic assumption of independence in inferential statistical tests (Hurlbert 1984). Due to this limitation, statistical analyses of recorded echoes were limited to descriptive statistics. For maximum peak amplitude and mean Wiener entropy, we calculated the average value in each day from 6 trials containing 5 repeated measures each. Thus, a total of 30 repeated measures were averaged to form a single daily measurement for each response variable for each angle-call-surface combination (n = 3). Grand means ± SE were presented for maximum peak amplitude and mean Wiener entropy.

For temporal waveform variation, we recorded once using the Y-jack in each trial, so 6 repeated measures in each day were averaged to form a single daily measurement for each angle-call-surface combination, except for the painted-painted comparison, in which 5 repeated measures in each day were averaged (n = 3 for each comparison). Grand means ± SE were presented for temporal waveform variation. Means were presented for normalized temporal waveform variation (n = 3 for each comparison). Normalized temporal waveform variation was also pooled across all calls at each angle and presented as grand means ± SD.

RESULTS

In total, we recorded 44,712 echoes (23 synthetic calls x 6 experimental surfaces x 6 trials x 6 repeated measures per trial x 3 angles x 3 days). Of these, we recorded 37,260 without the Y-jack and analyzed amplitude and spectral features for only these echoes (n=3 for each angle-call-surface combination). We recorded the remaining 7,452 echoes with the Y-jack, and only analyzed temporal modulation in these echoes (n=3 for each angle-call-surface combination). We examined the data for differences between surfaces in maximum peak amplitude, mean Wiener entropy, and temporal waveform variation of echoes (see Appendices E-J for tables of complete results).

Synthetic FM Sweeps — 0° Angle

At a 0° angle, we found no discernable maximum peak amplitude or mean Wiener entropy differences between echoes returning from playback of FM sweeps directed at smooth and textured surfaces. Nevertheless, we found that temporal waveform variation differed between surfaces when FM sweeps were above 40 kHz. For each FM sweep above 40 kHz, except for the 80-70 kHz sweep, we observed an increase in temporal waveform variation along the texture gradient from fine to coarse texture (Fig. 10). For the 80-70 kHz sweep, the medium texture exhibited the greatest temporal waveform variation (mean ± SE = 20.9 ± 19.0) and the unpainted smooth surface exhibited the second greatest temporal waveform variation (mean ± SE = 15.4 ± 14.1); however, these differences were not consistent across all trials and were potentially caused by an artifact of our experimental surface.

Pooled across FM sweeps for which we observed differences in temporal waveform variation between smooth and textured surfaces, normalized temporal waveform variation among the three potential wind turbine textures was greater for coarse texture (mean ± SD = 3.4 ± 1.5) than for medium texture (mean ± SD = 2.6 ± 1.2), and least pronounced for fine texture (mean ± SD = 1.8 ± 0.8). Among FM sweeps that displayed differences in temporal waveform variation, the effect of surface texture on

normalized temporal waveform variation also differed in magnitude (Fig. 11). We observed no discernable effect of surface texture on temporal waveform variation for synthetic FM sweeps with frequencies below 40 kHz.

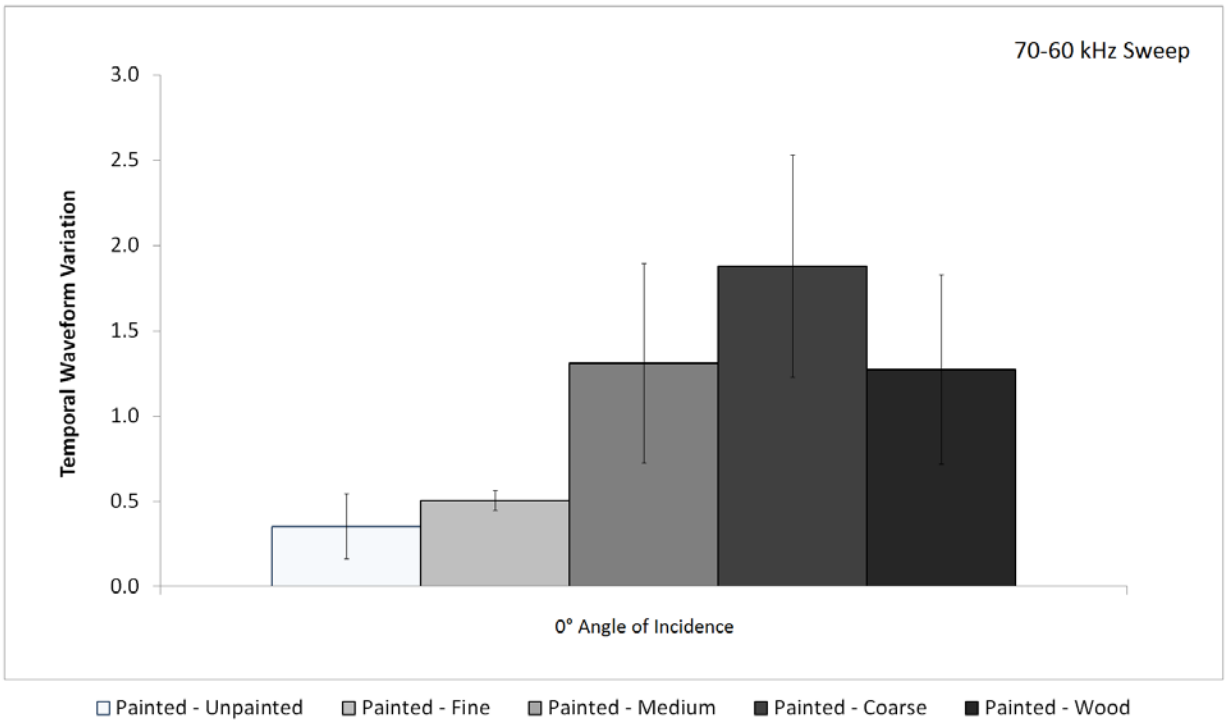

Figure 10. Mean ± SE (n = 3) temporal waveform variation (a. u., wherein higher values indicate greater temporal modulation differences) for 70-60 kHz synthetic FM sweep echoes reflecting off of the six surfaces at 0°. The effect of texture on temporal waveform variation at this frequency is representative of echoes returning from FM sweeps above 40 kHz.

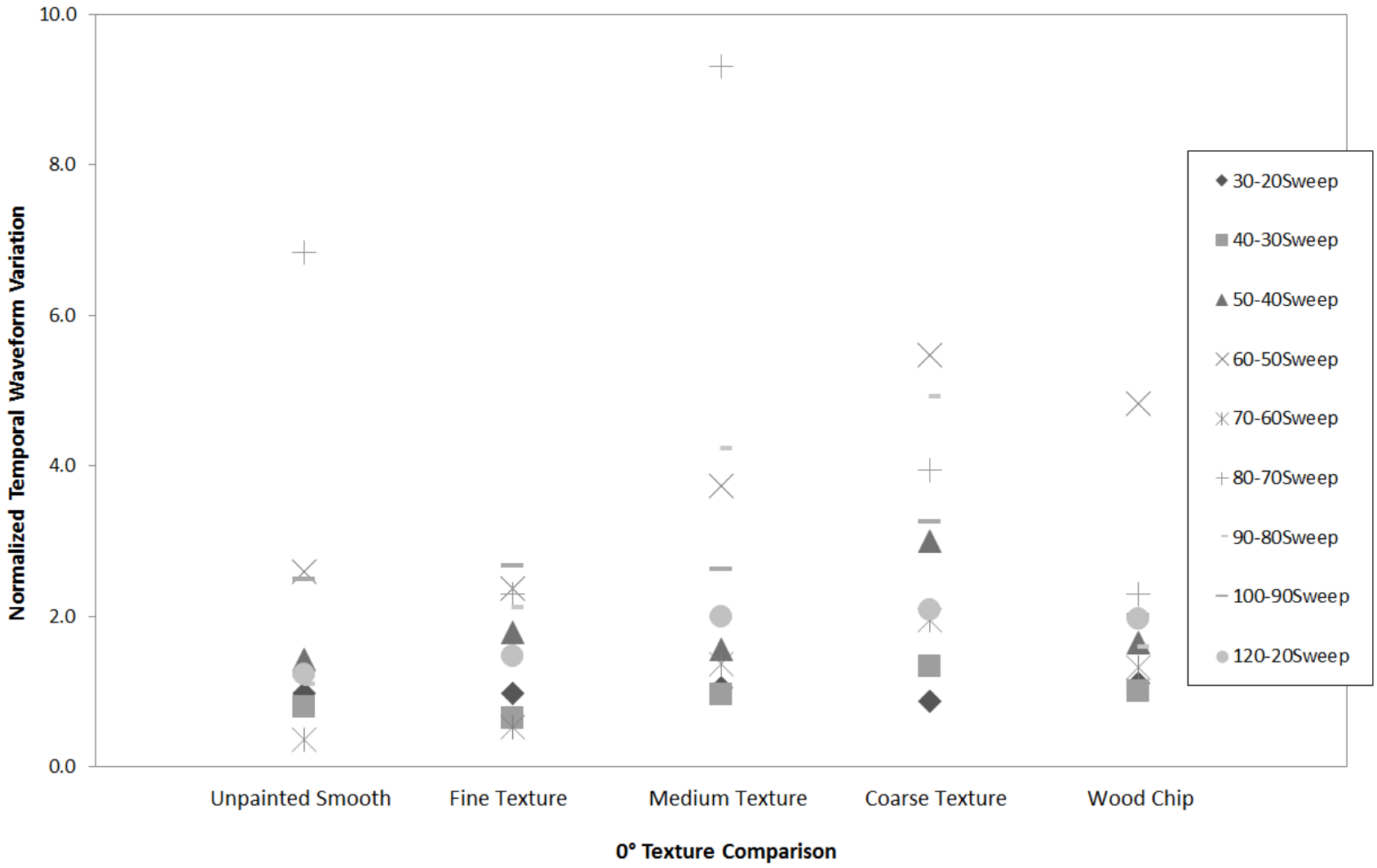

Figure 11. Mean normalized temporal waveform variation (n = 3 for each data point) for each texture comparison for the nine synthetic FM sweeps at 0°.

Synthetic Bat Calls — 0° Angle

At a 0° angle, we observed the same patterns for synthetic bat calls that we observed for synthetic FM sweeps >40 kHz. Effects of surface texture on temporal waveform variation were also similar between approach calls and terminal buzz calls. For each synthetic bat call, we observed an increase in temporal waveform variation along the texture gradient from fine to coarse texture (Fig. 12).

Pooled across all terminal buzz calls, normalized temporal waveform variation among the three potential wind turbine textures was greater for coarse texture (mean ± SD = 2.4 ± 0.5) than for medium texture (mean ± SD = 1.4 ± 0.4), while the normalized temporal waveform variation for fine texture was equivalent to those of smooth surfaces (mean ± SD = 1.0 ± 0.3). The effect of surface texture on normalized temporal waveform variation also differed in magnitude across terminal buzz calls (Fig. 13).

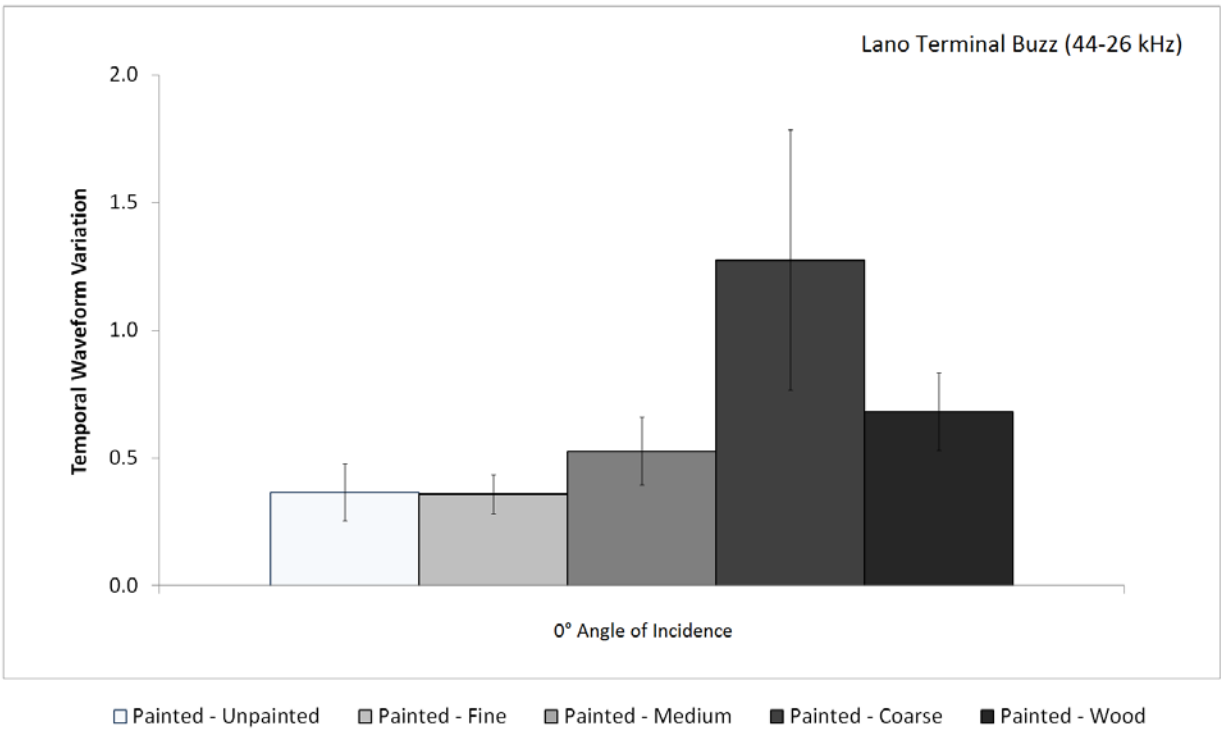

Figure 12. Mean ± SE (n = 3) temporal waveform variation (a. u., wherein higher values indicate greater temporal modulation differences) for 44-26 kHz (Lano terminal buzz) synthetic bat call echoes reflecting off of the six surfaces at 0°. The effect of texture on temporal waveform variation at this frequency is representative of echoes from synthetic bat calls.

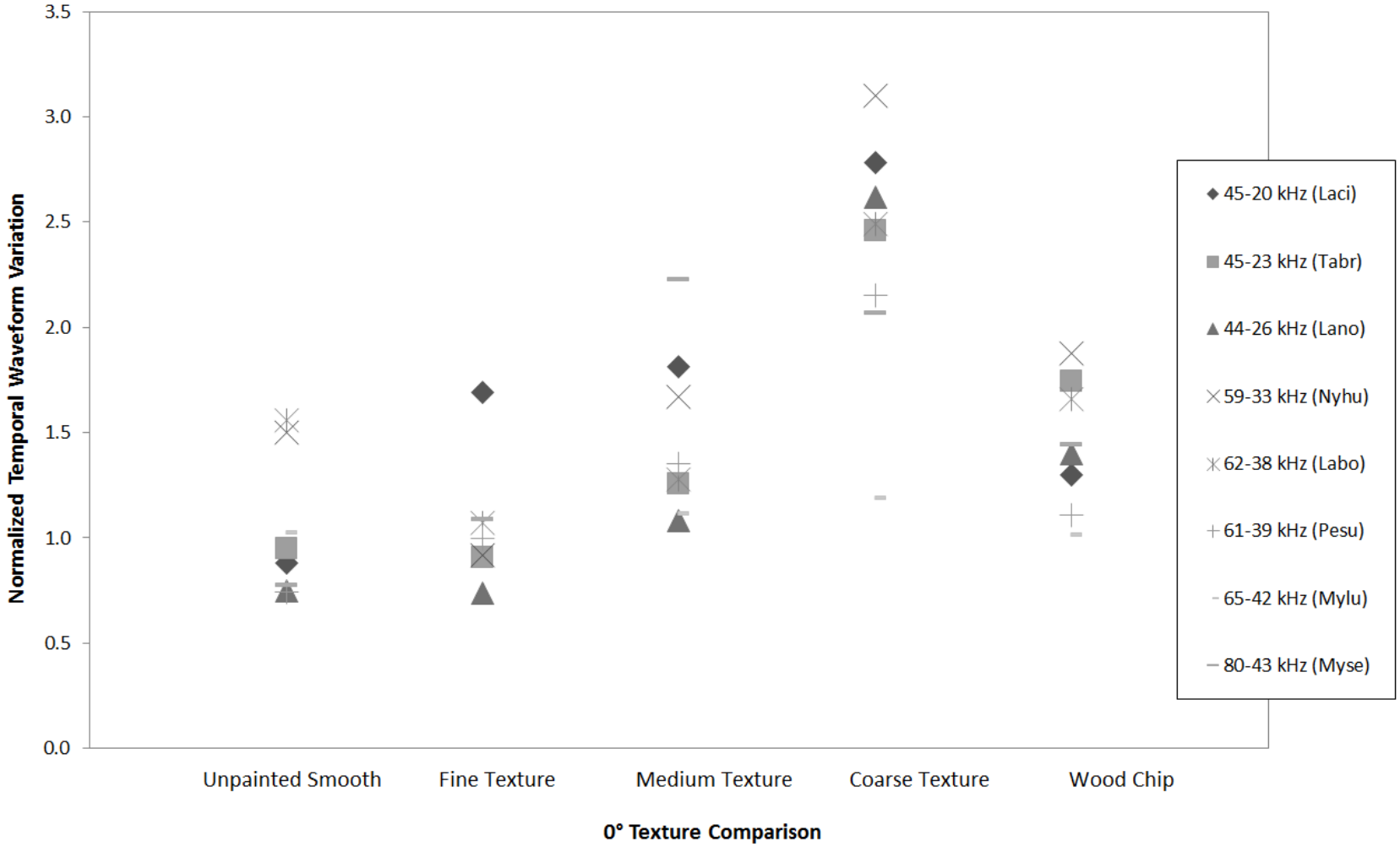

Figure 13. Mean normalized temporal waveform variation (n = 3 for each data point) for each texture comparison for the eight terminal buzz source calls at 0°.

Synthetic FM Sweeps — 20° Angle

At a 20° angle, we found that maximum peak amplitude differed by as much as 10 dB SPL (3-fold change in sound pressure) between echoes returning from playback of FM sweeps directed at smooth and textured surfaces when FM sweeps were above 50 kHz. For each FM sweep above 50 kHz, maximum peak amplitude increased along the texture gradient from fine to coarse texture (Fig. 14). This increased amplitude was likely due to the increased echo energy returning from direct and indirect reflections from the ridges on textured surfaces (i.e., scattering). We found no maximum peak amplitude differences among surface types for synthetic FM sweeps with frequencies below 50 kHz. We likely did not observe maximum peak amplitude differences among surface types at these frequencies because as frequency decreases, the ultrasonic source call becomes less directional (Mogensen and Møhl 1979). The broader radiation of sound would have caused more of the echo energy to return from a steeper angle (i.e., nearer to 0° rather than 20°), resulting in minimal amplitude effects induced by surface texture.

We also found that mean Wiener entropy differed between echoes returning from playback of FM sweeps directed at smooth and textured surfaces. For FM sweeps above 70 kHz, we found that mean Wiener entropy decreased along the texture gradient from fine to coarse texture (Fig. 15). This likely occurred because the increased echo energy reflecting off of textured surfaces contributed to a higher signal-to-noise ratio, reducing the spectral flatness of the echo. For FM sweeps below 70 kHz (except for the 50-40 kHz sweep), the pattern was reversed, and mean Wiener entropy increased along the texture gradient from fine to coarse texture (Fig. 16). This likely occurred due to a combination of factors. First, scattering of echo energy from textures contributed to increased spectral disorder, increasing mean Wiener entropy. Second, these lower frequencies were less directional, causing signal-to-noise ratios of echoes reflecting off of smooth and textured surfaces to be similar.

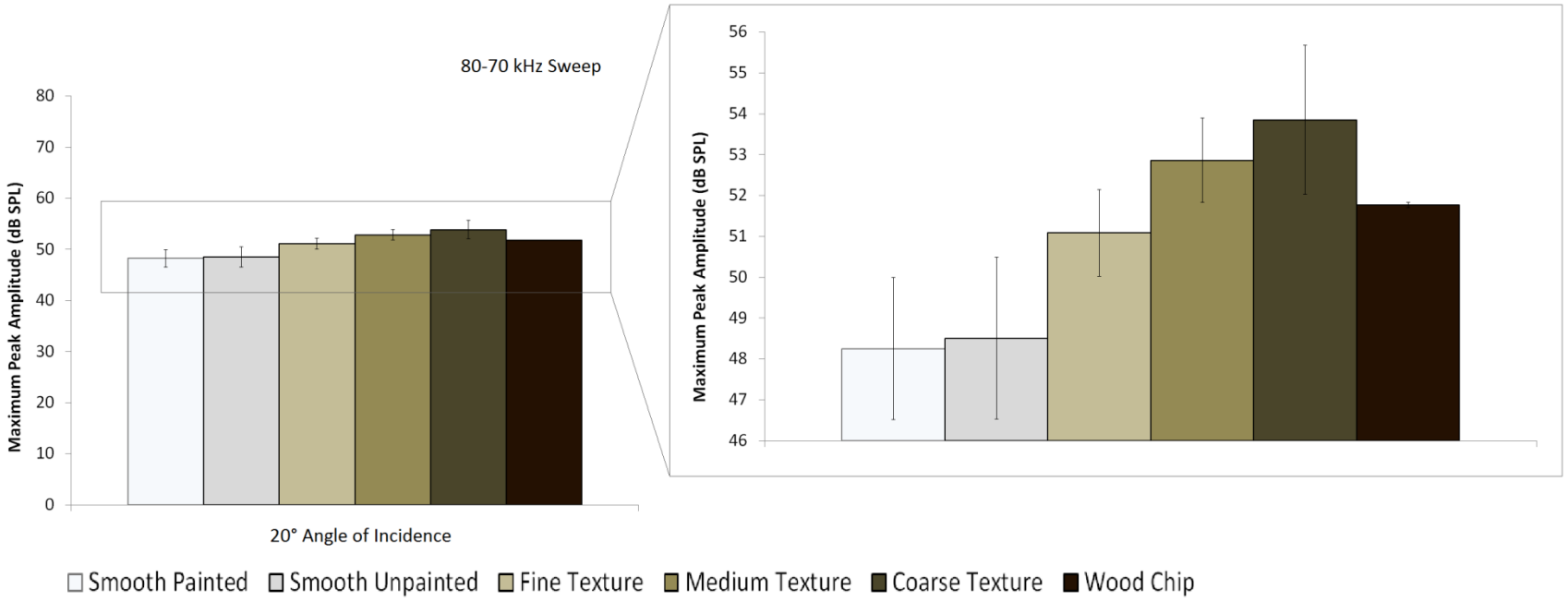

Figure 14. Mean ± SE (n = 3) maximum peak amplitude (dB SPL) for 80-70 kHz synthetic FM sweep echoes reflecting off of the six surfaces at 20°. Maximum peak amplitude increased along the texture gradient for FM sweeps containing frequencies above 40 kHz.

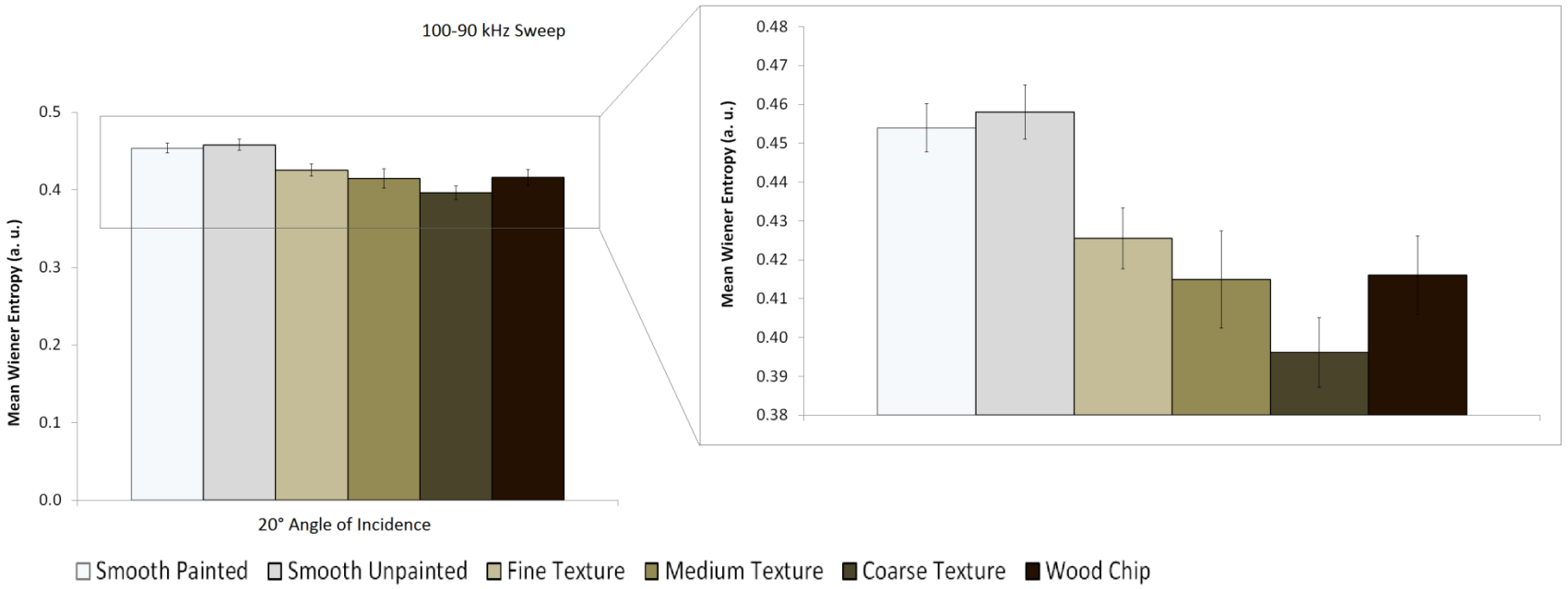

Figure 15. Mean ± SE (n = 3) mean Wiener entropy (a. u., wherein 0 represents a pure tone and 1 represents white noise) for 100-90 kHz synthetic FM sweep echoes reflecting off of the six surfaces at 20°. Mean Wiener entropy decreased along the texture gradient for synthetic FM sweeps above 70 kHz.

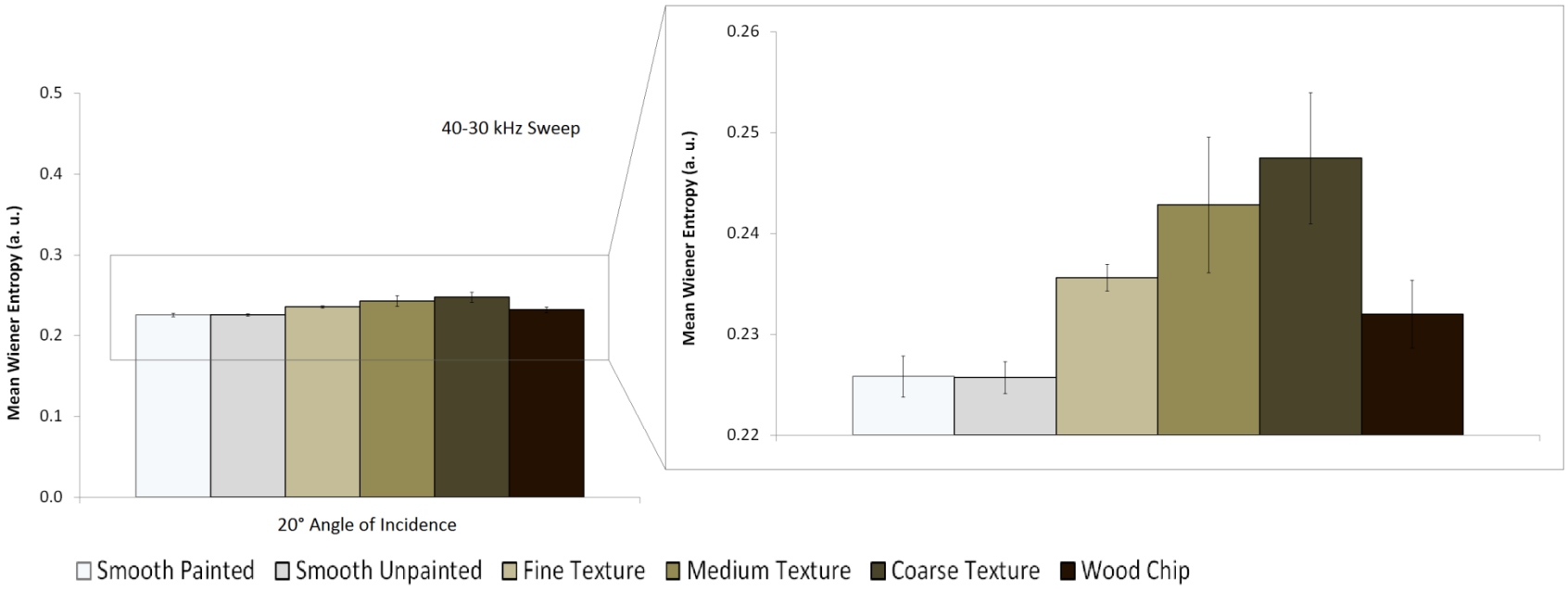

Figure 16. Mean ± SE (n = 3) mean Wiener entropy (a. u., wherein 0 represents a pure tone and 1 represents white noise) for 40-30 kHz synthetic FM sweep echoes reflecting off of the six surfaces at 20°. Mean Wiener entropy increased along the texture gradient for FM sweeps with frequencies below 70 kHz.

We generally observed an increase in temporal waveform variation for all FM sweeps along the texture gradient from fine to coarse texture. Exceptions to this pattern were the 100-90 kHz sweep (for which medium texture exhibited the highest temporal waveform variation) and the 90-80 kHz sweep (for which fine texture exhibited slightly higher temporal waveform variation than the medium texture; Fig. 17). For these two FM sweeps, we observed more similar values for temporal waveform variation of fine, medium, and coarse texture than for FM sweeps below 80 kHz. Pooled across FM sweeps, normalized temporal waveform variation among the three potential wind turbine textures was greater for coarse texture (mean ± SD = 19.2 ± 18.9) than for medium texture (mean ± SD = 7.4 ± 3.9), and was least pronounced for fine texture (mean ± SD = 5.0 ± 2.7). The effect of surface texture on normalized temporal waveform variation differed in magnitude across FM sweeps (Fig. 18). We also observed an increase in magnitude of temporal waveform variation with increasing frequency (Fig. 19).

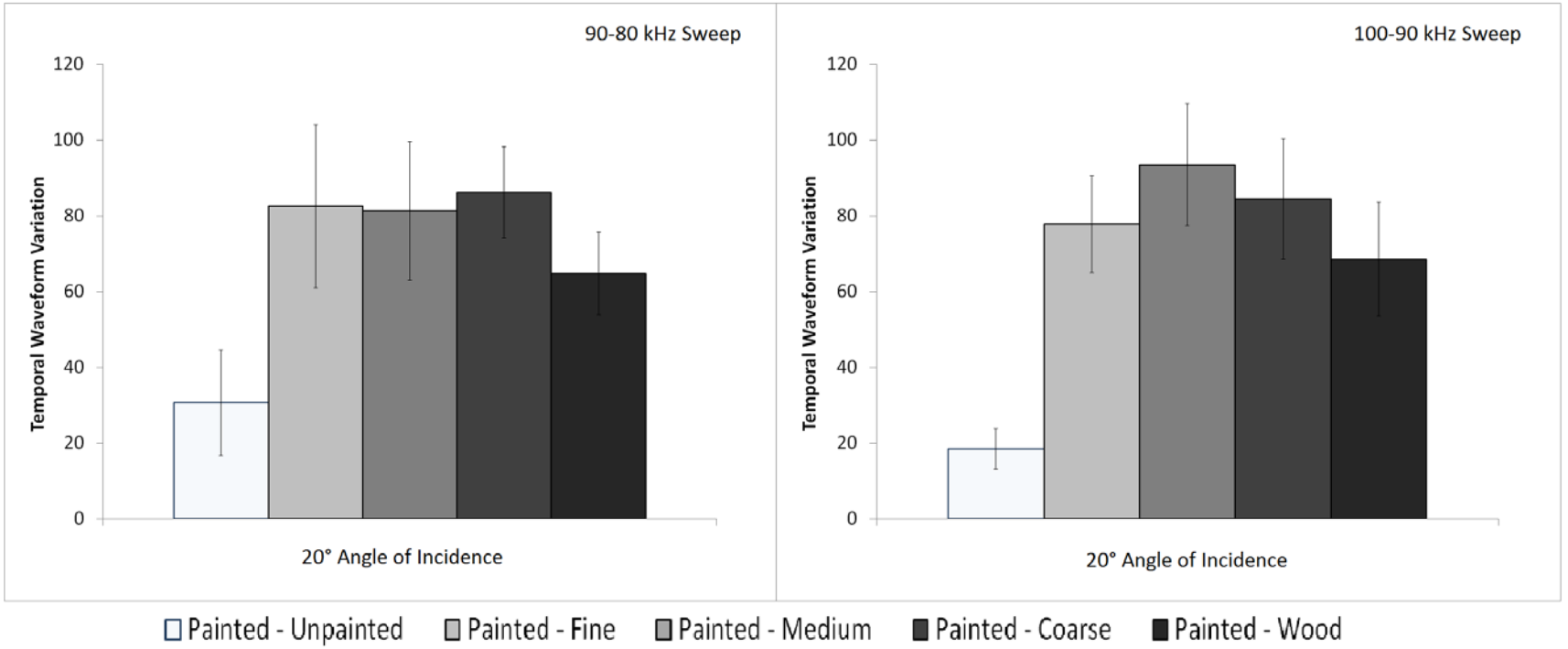

Figure 17. Mean ± SE (n = 3) temporal waveform variation (a. u., wherein higher values indicate greater temporal modulation differences) for 90-80 and 100-90 kHz synthetic FM sweep echoes reflecting off of the six surfaces at 20°. At source call frequencies above 80 kHz, temporal waveform variation was more similar between painted-fine, painted-medium, and painted-coarse textures than at source call frequencies below 80 kHz.

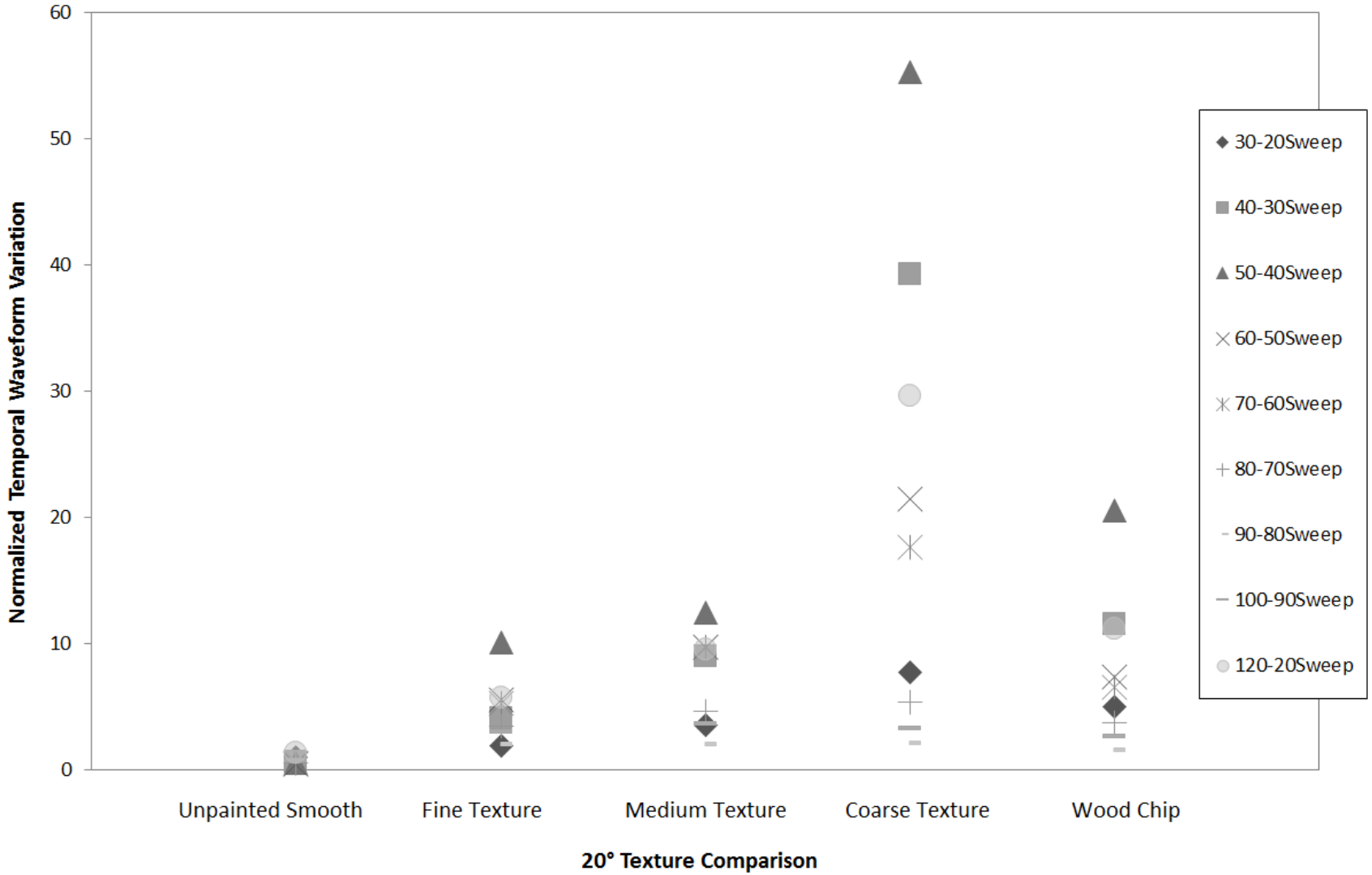

Figure 18. Mean normalized temporal waveform variation (n = 3 for each data point) for each texture comparison for the nine synthetic FM sweeps at 20°.

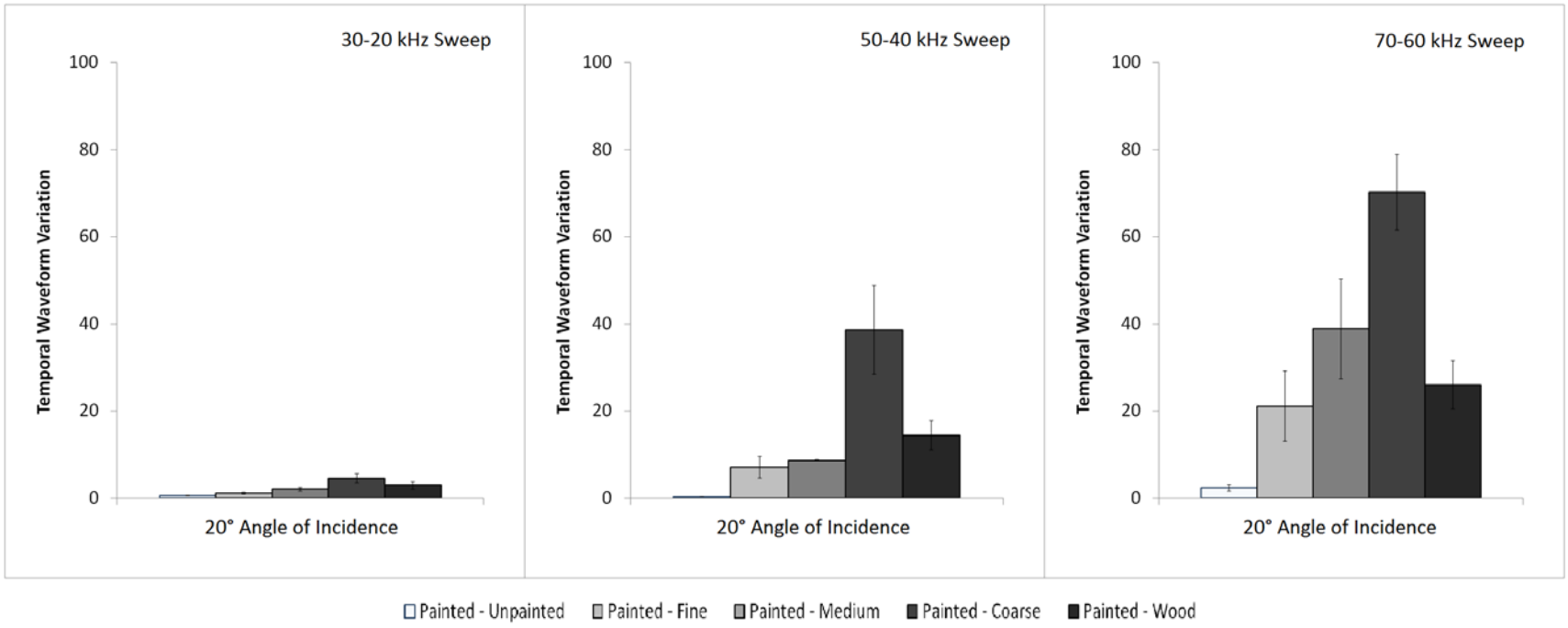

Figure 19. Mean ± SE (n = 3) temporal waveform variation (a. u., wherein higher values indicate greater temporal modulation differences) for 30-20, 50-40, and 70-60 kHz synthetic FM sweep echoes reflecting off of the six surfaces at 20°. The magnitude of temporal waveform variation increased as source call frequency increased.

Synthetic Bat Calls — 20° Angle

At a 20° angle, we found that maximum peak amplitude differed between echoes returning from playback of synthetic bat calls directed at smooth and textured surfaces for the Myse terminal buzz call (80-43 kHz). For this synthetic bat call, maximum peak amplitude increased along the texture gradient by up to 3 dB SPL (1.4-fold increase in sound pressure). We observed no other discernable differences in maximum peak amplitude between echoes returning from playback of synthetic bat calls directed at smooth and textured surfaces for either approach or terminal buzz calls. The absence of amplitude differences between smooth and textured surfaces for the remainder of our synthetic bat calls was consistent with the results we obtained for FM sweeps as most of the call energy contained within the remaining synthetic bat calls was below 50 kHz.

Mean Wiener entropy for synthetic bat calls exhibited the same pattern as that observed for the synthetic FM sweeps with frequencies below 70 kHz, increasing along the texture gradient from fine to coarse texture (Fig. 20). We also found that temporal waveform variation increased along the texture gradient from fine to coarse texture for all synthetic bat calls. Pooled across terminal buzz calls, normalized temporal waveform variation among the three potential wind turbine textures was greater for coarse texture (mean ± SD = 34.7 ± 14.3) than for the medium texture (mean ± SD = 10.4 ± 5.9), and was least pronounced for fine texture (mean ± SD = 4.9 ± 2.5). The effect of surface texture on normalized temporal waveform variation also differed in magnitude across source calls (Fig. 21). As with the synthetic FM sweeps, the magnitude of temporal waveform variation also increased with increasing frequency of the source calls.

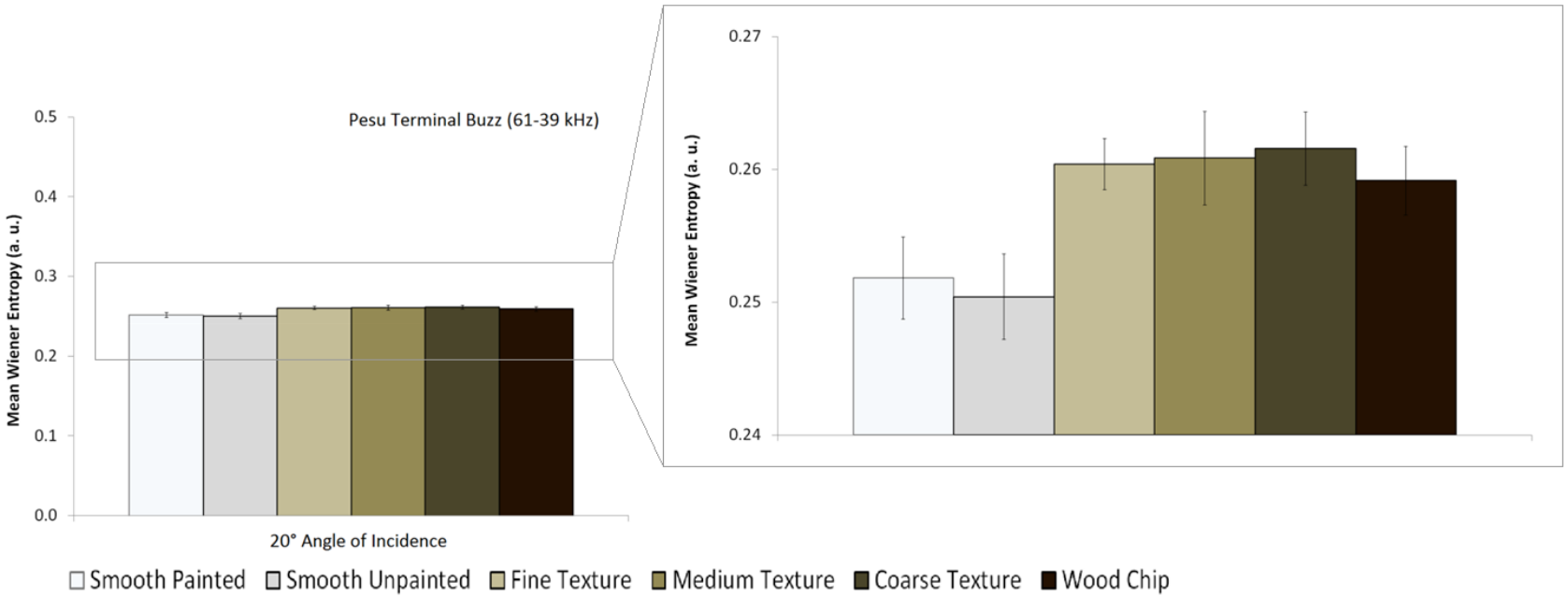

Figure 20. Mean ± SE (n = 3) mean Wiener entropy (a. u., wherein 0 represents a pure tone and 1 represents white noise) for 61-39 kHz (Pesu terminal buzz) synthetic bat call echoes reflecting off of the six surfaces at 20°. Mean Wiener entropy increased along the texture gradient for synthetic bat calls.

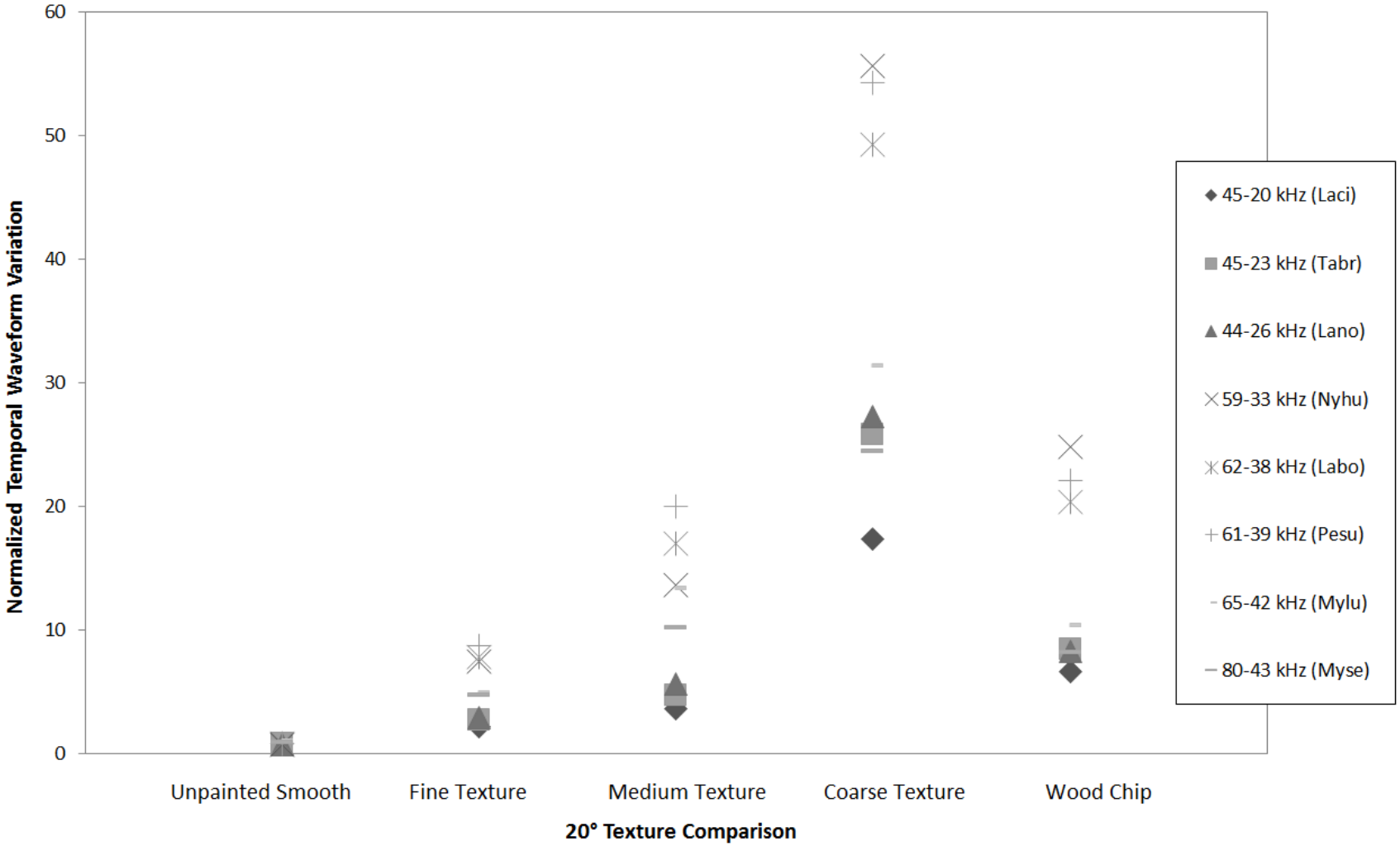

Figure 21. Mean normalized temporal waveform variation (n = 3 for each data point) for each texture comparison for the eight terminal buzz source calls at 20°.

Synthetic FM Sweeps — 40° Angle

At a 40° angle, we found that maximum peak amplitude differed by as much as 19 dB SPL (9-fold difference in sound pressure) between echoes returning from playback of FM sweeps directed at smooth and textured surfaces when FM sweeps were above 30 kHz. For each FM sweep above 30 kHz, maximum peak amplitude increased along the texture gradient from fine to coarse texture (Fig. 22). This increased amplitude was likely caused by the same mechanism at 40° as at it was at 20° (i.e., increased echo energy returning to the microphone due to acoustic scattering from textures). We found no maximum peak amplitude differences between smooth and textured surfaces for the 30-20 kHz FM sweep which was, once again, likely because the lower frequency source call was less directional causing the highest echo intensity to return from the 0° angle, despite this being 40° off-axis.

We found that mean Wiener entropy also differed between echoes returning from playback of FM sweeps directed at smooth and textured surfaces, likely for the same reasons that it differed among surfaces at 20°. For FM sweeps above 30 kHz, mean Wiener entropy decreased along the texture gradient from fine to coarse texture (Fig. 23). For the 30-20 kHz sweep, we observed the reverse pattern, as mean Wiener entropy increased along the texture gradient from fine to coarse texture (Fig. 24).

We were unable to analyze the 80-70 kHz and 50-40 kHz FM sweeps for temporal waveform variation because many of the echoes returning from playback of these FM sweeps directed at the smooth surfaces were of such low amplitude that echo could not be distinguished from ambient noise in the sound studio. For all FM sweeps that we were able to analyze, except the 40-30 kHz sweep, we observed an increase in temporal waveform variation along the texture gradient from fine to coarse texture. For the 40-30 kHz sweep, temporal waveform variation was greatest for the medium texture. Pooled across analyzable FM sweeps, normalized temporal waveform variation among the three potential wind turbine textures was slightly greater for coarse texture (mean ± SD = 14.3 ± 13.8) than for

medium texture (mean ± SD = 12.8 ± 12.2), and was slightly less pronounced for fine texture (mean ± SD = 12.1 ± 11.1). The effect of surface texture on normalized temporal waveform variation also differed in magnitude across FM sweeps (Fig. 25). Among FM sweeps, normalized temporal waveform variations for textured surfaces were lower at 40° than at 20°; however, temporal waveform variation magnitudes were much larger at 40° than at 20° for all textured surfaces (Fig. 26).

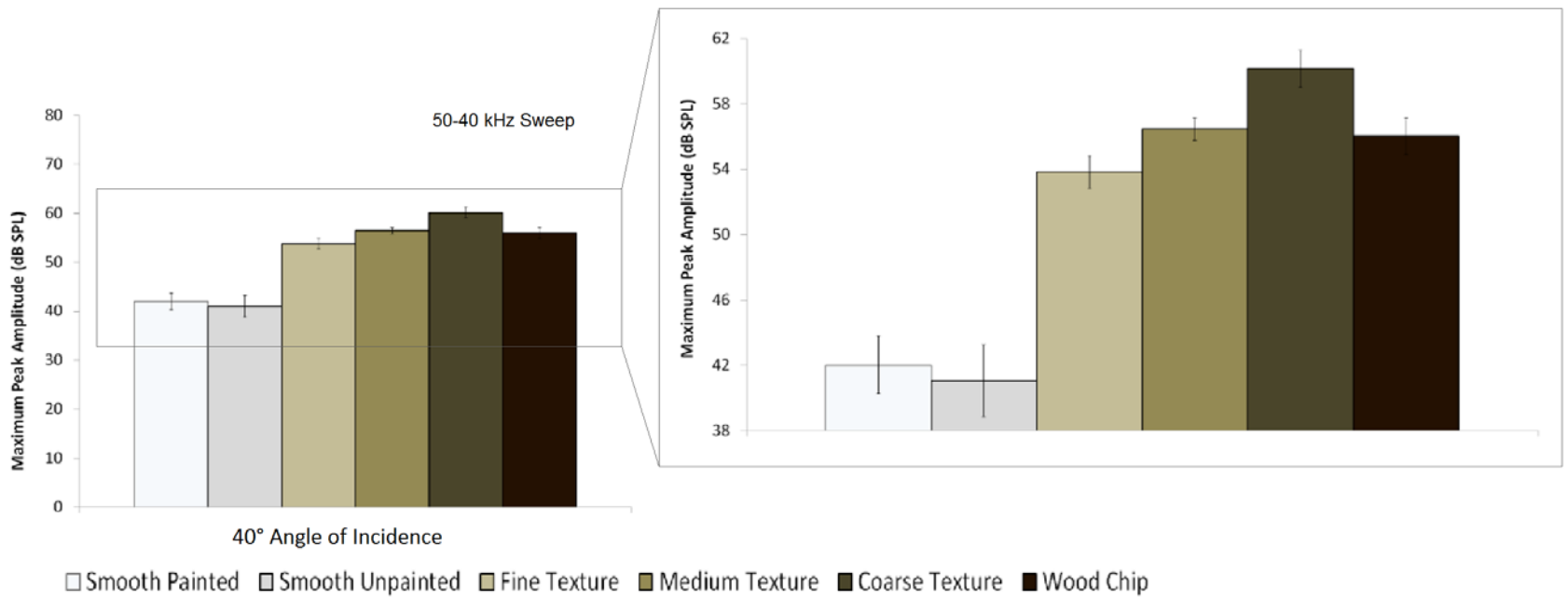

Figure 22. Mean ± SE (n = 3) maximum peak amplitude (dB SPL) for 50-40 kHz synthetic FM sweep echoes reflecting off of the six surfaces at 40°. Maximum peak amplitude increased along the texture gradient for all FM sweeps except for the 30-20 kHz sweep.

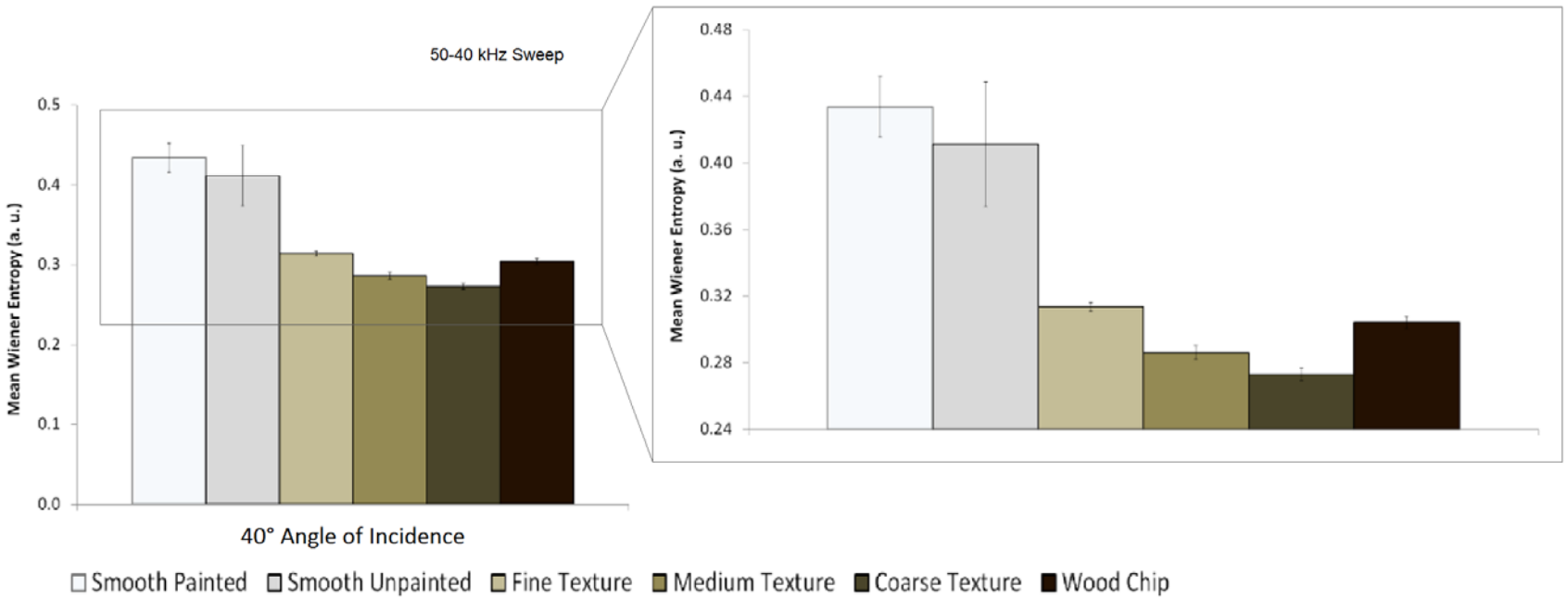

Figure 23. Mean ± SE (n = 3) mean Wiener entropy (a. u., wherein 0 represents a pure tone and 1 represents white noise) for 50-40 kHz synthetic FM sweep echoes reflecting off of the six surfaces at 40°. Mean Wiener entropy decreased along the texture gradient for all synthetic FM sweeps except the 30-20 kHz sweep.

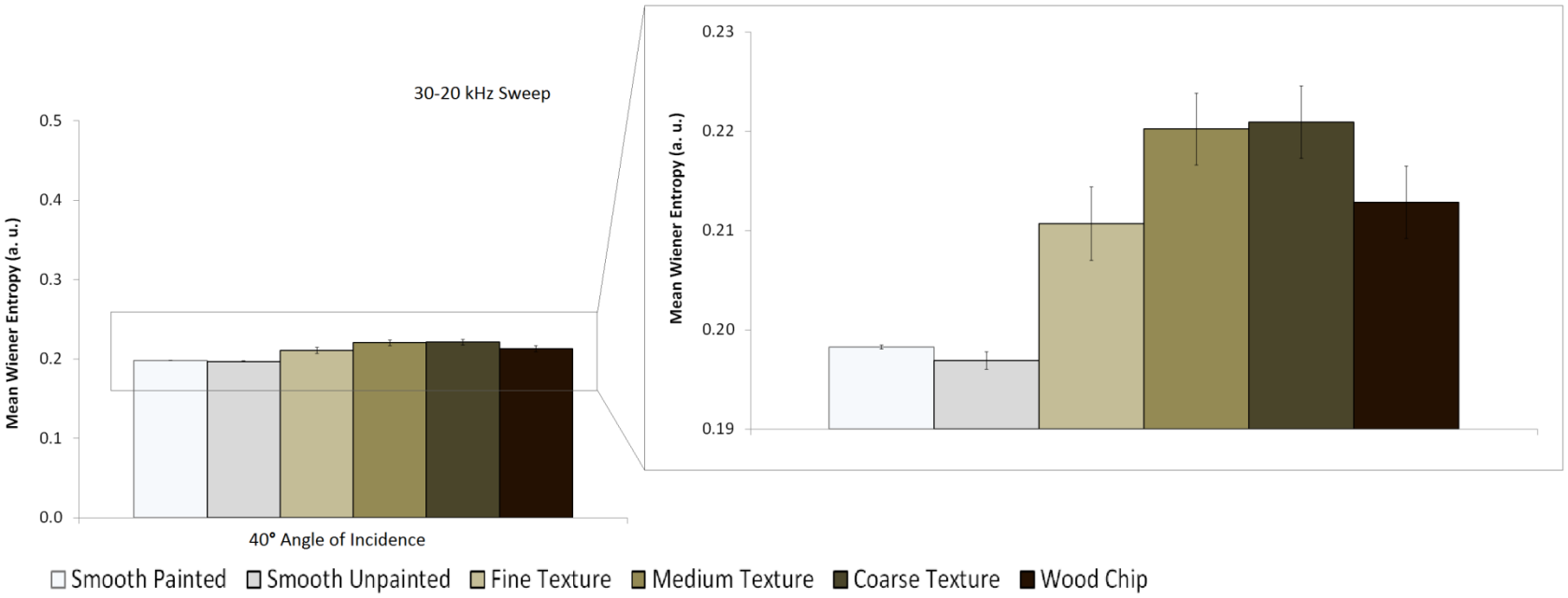

Figure 24. Mean ± SE (n = 3) mean Wiener entropy (a. u., wherein 0 represents a pure tone and 1 represents white noise) for 30-20 kHz synthetic FM sweep echoes reflecting off of the six surfaces at 40°. Mean Wiener entropy increased along the texture gradient at this frequency.

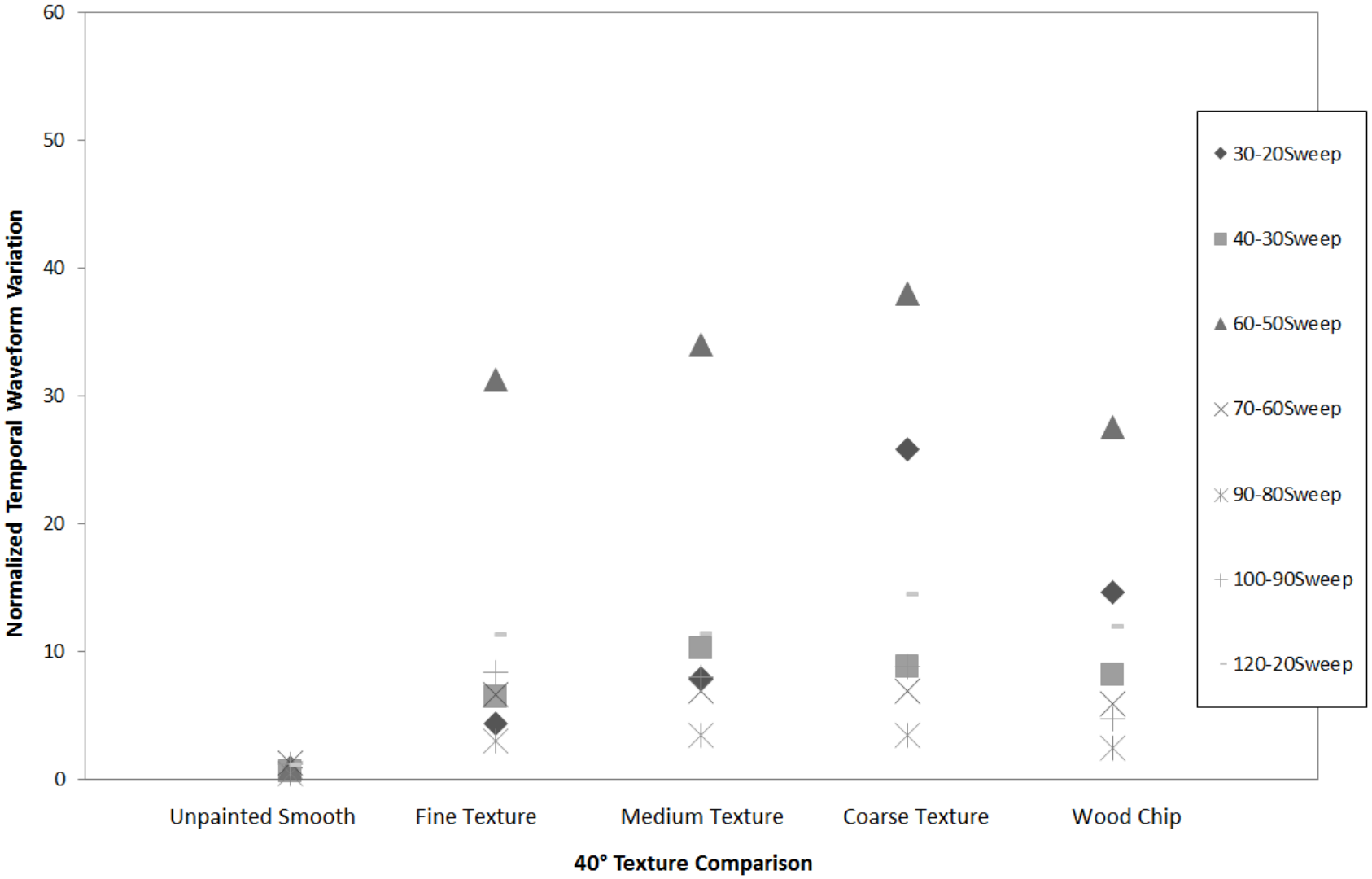

Figure 25. Mean normalized temporal waveform variation (n = 3 for each data point) for each texture comparison for the seven synthetic FM sweeps at 40° for which temporal waveform analysis was possible.

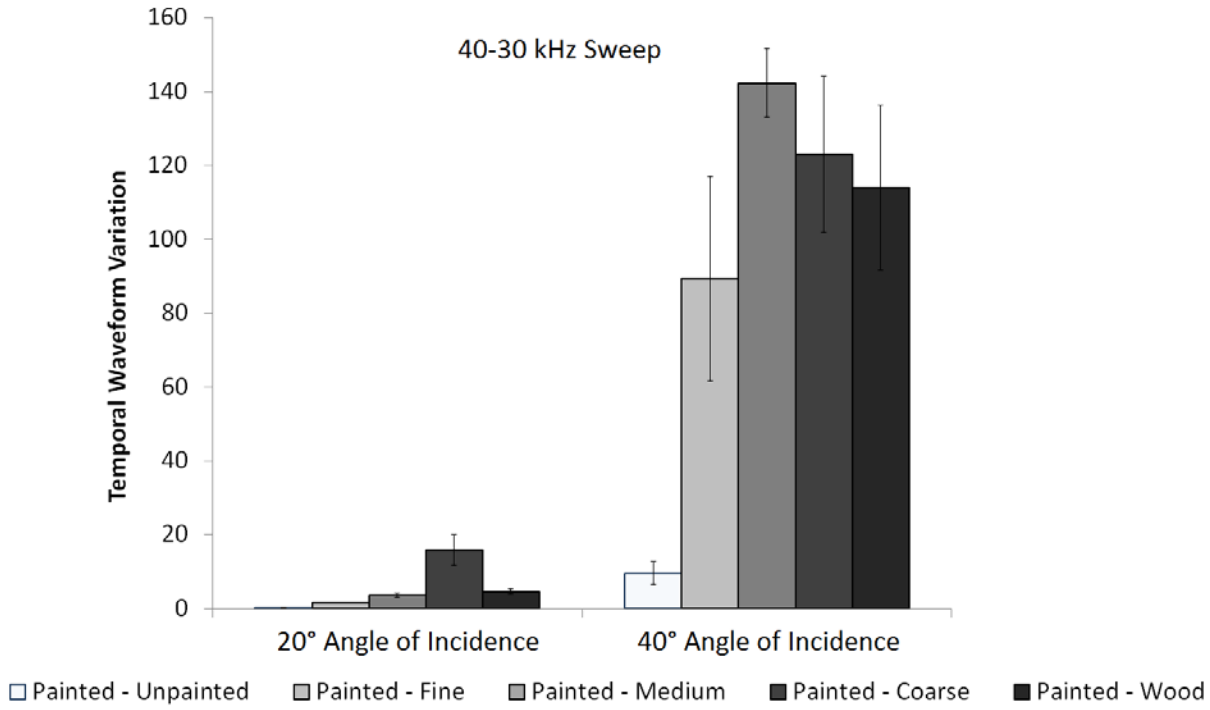

Figure 26. Mean ± SE (n = 3) temporal waveform variation (a. u., wherein higher values indicate greater temporal modulation differences) for 40-30 kHz synthetic FM sweep echoes reflecting off of the six surfaces at 20° and 40°. The magnitude of temporal waveform variation increased greatly as angle of incidence became shallower.

Synthetic Bat Calls — 40° Angle

At a 40° angle, we found that maximum peak amplitude differed between echoes returning from playback of synthetic bat calls directed at smooth and textured surfaces for the Myse, Mylu, and Lano terminal buzz calls, and both approach and terminal buzz calls for Pesu, Labo, and Nyhu. For these synthetic bat calls, we observed that maximum peak amplitude of echoes increased along the texture gradient from fine to coarse texture. Maximum peak amplitude differed between smooth and textured surfaces by as much as 21 dB SPL (11-fold increase in sound pressure). For the Lano approach call, and approach and terminal buzz calls for Laci and Tabr, we found no discernable maximum peak amplitude differences between smooth and textured surfaces. These results were comparable to what we

observed for synthetic FM sweeps occupying similar frequency ranges, as the low frequency synthetic bat calls (Laci, Tabr, and Lano) contain frequencies below 30 kHz.

We found that mean Wiener entropy differed between echoes returning from playback of all synthetic bat calls directed at smooth and textured surfaces. For synthetic bat calls with frequency ranges above 30 kHz (Myse and Mylu terminal buzz calls, and both approach and terminal buzz calls for Pesu, Labo, and Nyhu) mean Wiener entropy decreased along the texture gradient from fine to coarse texture. For the Laci, Tabr, and Lano approach calls, we observed an increase in mean Wiener entropy along the texture gradient from fine to coarse texture. For the Laci, Tabr and Lano terminal buzz calls, mean Wiener entropy was higher for textured surfaces than for smooth surfaces; yet for these synthetic bat calls, we observed a decrease in mean Wiener entropy along the texture gradient from fine to coarse texture. This pattern was likely observed because the frequencies of these synthetic bat calls were at the transition between increasing Wiener entropy with increasing texture particle size and decreasing Wiener entropy with increasing texture particle size. Overall, patterns in mean Wiener entropy of echoes reflecting off of smooth and textured surfaces were comparable to what we observed for synthetic FM sweeps occupying similar frequency ranges.

We observed an increase in temporal waveform variation along the texture gradient from fine to coarse texture for all synthetic bat calls. Pooled across all terminal buzz calls, normalized temporal waveform variation among the three potential wind turbine textures was greater for coarse texture (mean ± SD = 59.3 ± 59.9) than for medium texture (mean ± SD = 33.2 ± 28.5) and least pronounced for fine texture (mean ± SD = 16.8 ± 9.5). The effect of surface texture on normalized temporal waveform variation also differed in magnitude across synthetic bat calls (Fig. 27).

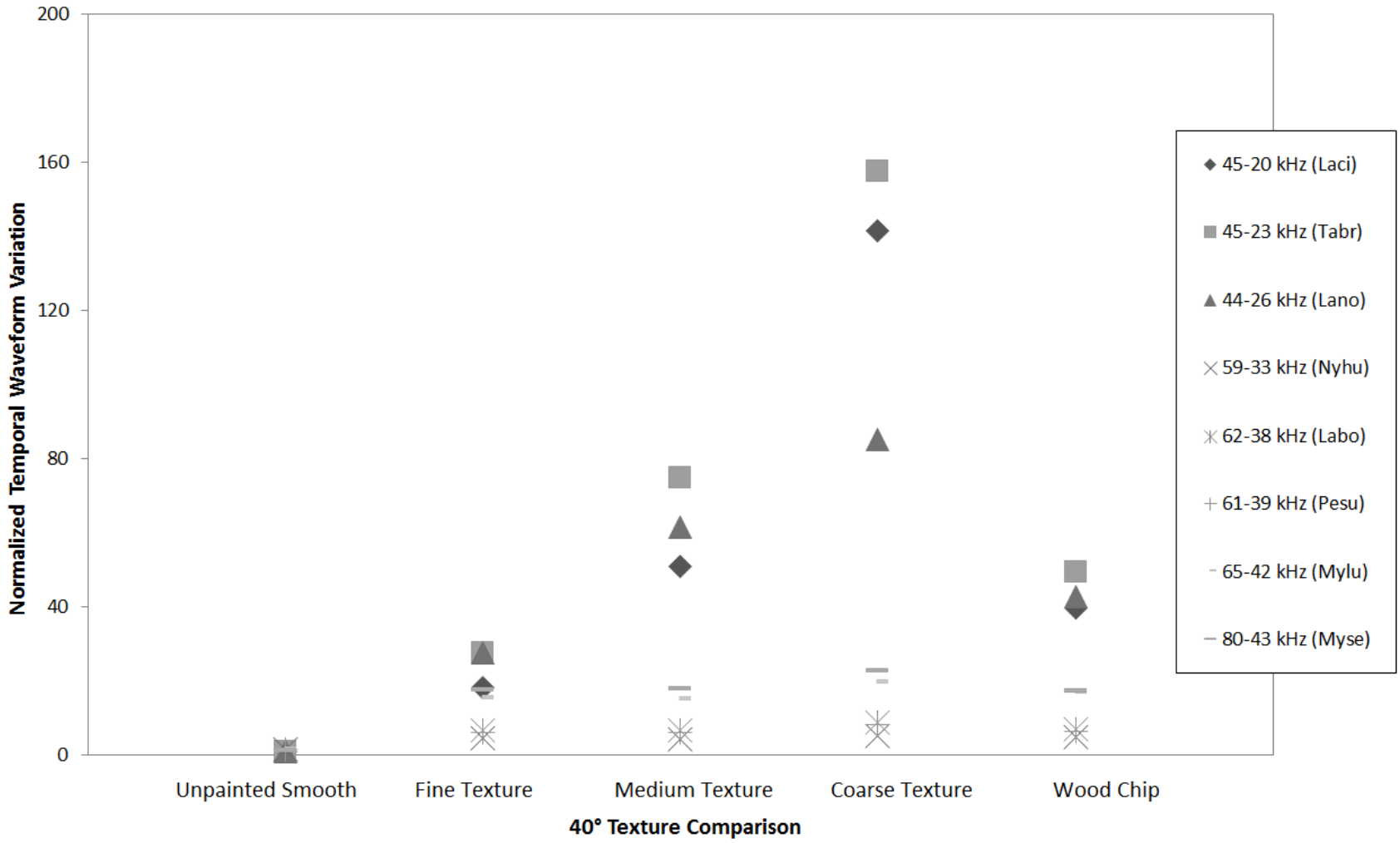

Figure 27. Mean normalized temporal waveform variation (n = 3 for each data point) for each texture comparison for the eight terminal buzz source calls at 40°.

DISCUSSION

The results of our playback experiment revealed acoustic differences between echoes reflecting off of smooth and textured surfaces in all three of our response variables, maximum peak amplitude, mean Wiener entropy, and temporal waveform variation. The extent of these differences did, however, depend on both angle of incidence and source call frequency. Across all experimental trials, smooth painted and smooth unpainted surfaces showed no discernable acoustic differences, consistent with the hypothesis proposed by McAlexander (2013) that water and wind turbine surfaces are acoustically similar. At angles of incidence and source call frequencies for which smooth and textured surfaces could be differentiated, the acoustic differences tended to be more pronounced for echoes reflecting off of textures with larger particle sizes than for echoes reflecting off of textures with smaller particle sizes.

At a 0° angle of incidence, for source calls above 40 kHz, we found that temporal characteristics (i.e., temporal waveform variation) of echoes reflecting off of textured surfaces could be differentiated from those reflecting off of smooth surfaces. In contrast, intensity and spectral characteristics (i.e., maximum peak amplitude and mean Wiener entropy) could not be differentiated between surface types. Furthermore, the temporal differences were of small magnitude and there were no differences below 40 kHz. This result suggests that for low frequency bat species (we define low frequency bat species as species whose echolocation calls are typically below 35 kHz; i.e., hoary, Mexican free-tailed, and silver-haired bats) all textures in the gradient might be perceived to be smooth at 0°. A study on big brown bats (*Eptesicus fuscus*) demonstrated that they had the ability to resolve similar closely-overlapping echoes using only temporal cues (Simmons et al. 1998); however, it remains unclear whether bat species commonly killed at wind turbines are also able to differentiate surface texture using only temporal cues of small magnitude in the absence of intensity and spectral cues.

Although our results revealed greater acoustic differences between smooth and textured surfaces at shallower angles of incidence, our results at 0° may still be relevant, as bats approaching

wind turbine tower surfaces initially receive the majority of echo energy from the 0° angle (ca. 15 m and 40 m distance from the surface at first detection of the tower for 50 kHz and 20 kHz echolocation calls, respectively; Stilz and Schnitzler 2012). Nevertheless, as bats come closer to wind turbine towers, other angles of incidence will become available to them when inspecting the surfaces. Texture differentiation at these closer distances is also relevant as any reduction in the amount of time spent investigating wind turbines should reduce the amount of time spent within the rotor-swept zone, and thus the relative risk of collision.

As the angle of incidence becomes shallower, acoustic differences between smooth and textured surfaces become more pronounced, mainly due to increased acoustic energy resulting from scattering of echoes from textures (Fig. 28). Thus, at 20° and 40°, we observed acoustic differences between smooth and textured surfaces for all response variables that we investigated (maximum peak amplitude, mean Wiener entropy, and temporal waveform variation). For source calls with high frequencies (above 50 kHz at 20° and above 30 kHz at 40°), maximum peak amplitude of echoes increased along the texture gradient, yet showed no differences for source calls at all other frequencies. This result suggests that for high frequency bat species (we define high frequency bat species as species whose echolocation calls are typically above 35 kHz; i.e., northern long-eared, little brown, tri-colored, eastern red, and evening bats) textured surfaces could be differentiated from smooth surfaces using echo intensity information, especially at shallow angles. For source calls with high frequencies (above 70 kHz at 20° and above 30 kHz at 40°), mean Wiener entropy of echoes decreased along the texture gradient becoming closer to a pure tone. For source calls at all other frequencies (i.e., below 70 kHz at 20° and below 30 kHz at 40°), however, mean Wiener entropy increased along the texture gradient, becoming more chaotic. Thus, mean Wiener entropy results suggested that for both low and high frequency bat species, textured surfaces could be differentiated from smooth surfaces using echo spectral information at both 20° and 40°. Finally, for all source calls at 20° and 40°, temporal waveform

variation increased along the texture gradient and showed greater increases at higher frequencies, suggesting that textured surfaces could be differentiated by bats using echo temporal information across the range of frequencies at 20° and 40°.

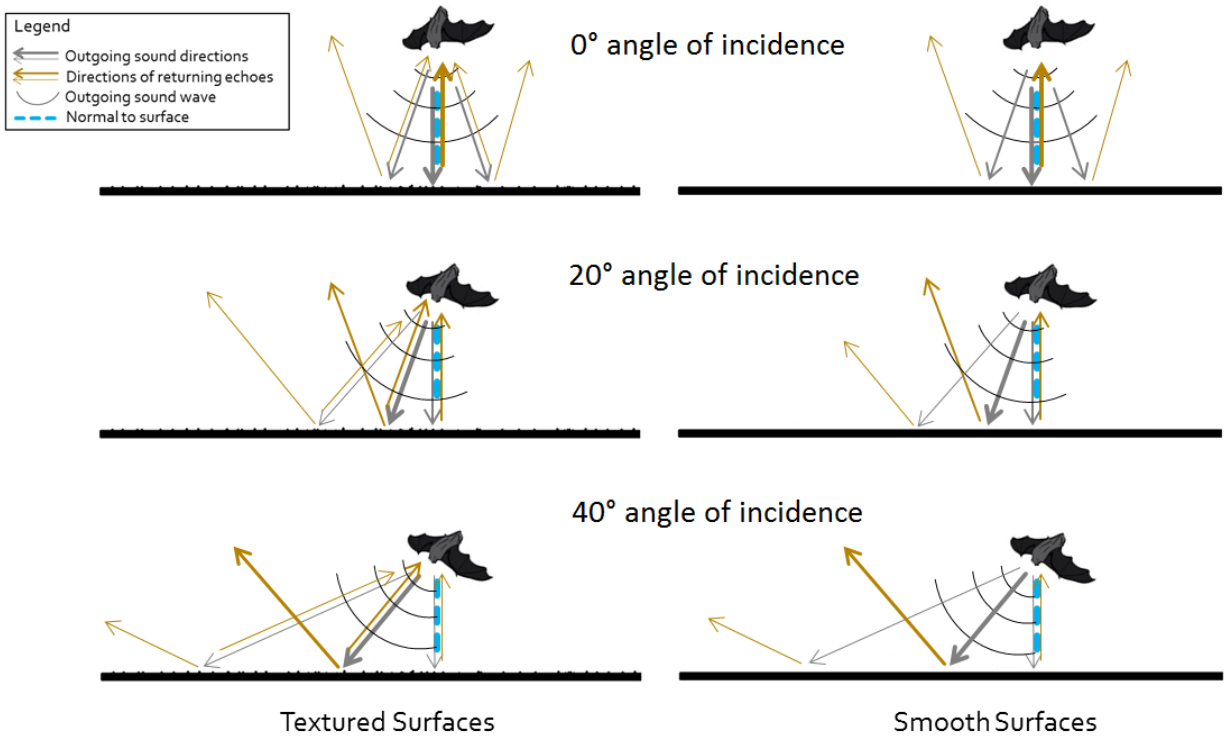

Figure 28. Simplified representation of echoes and representative echo energy reflected off of smooth and textured surfaces based on angle of incidence. Most of the sound energy is reflected back to the emitter at a 0° angle regardless of the surface texture. At a 20° angle, more of the energy is reflected back to the emitter through scattering from a textured surface compared to a smooth surface. At a 40° angle, some energy is reflected back to the emitter through scattering off of a textured surface, while almost all of the energy is reflected away from the emitter off of a smooth surface.

Together, these results suggest that when high frequency bat species investigate textured surfaces at very shallow angles, the echoes they receive are more intense, are of purer tone, and contain more energy arriving after the first reflections compared with echoes reflecting off of smooth surfaces. For low frequency bat species, echoes may or may not be more intense, but they are more chaotic, and

contain more energy arriving after the first reflections at the same angle of incidence.

Overall, these results support our hypothesis that adding texture additives (e.g., sand) as part of the wind turbine paint coating could alter the acoustic properties of wind turbine towers such that ultrasonic echoes returning from these modified towers could be differentiated from those returning from smooth surfaces. Additionally, many of the results that we obtained show clear stepwise increases in acoustic differences between smooth and textured surfaces along the texture gradient from smooth to coarse texture, supporting our additional hypothesis that the addition of texture additives with larger particle sizes results in greater acoustic differences from smooth surfaces.

We also noted that for higher frequency source calls (e.g., the 70-60 kHz FM sweep), the medium and fine textures produced echoes that were nearly as distinct from smooth surfaces as the coarse texture. Based on this pattern, high frequency bat species may not require large particle sizes to effectively differentiate between smooth and textured surfaces in comparison to low frequency bat species. As bats adapted to foraging in cluttered environments typically use high frequency echolocation calls to gain more information about their immediate surroundings, this finding is not unexpected (Schmieder et al. 2012). If only high frequency bat species were present, texturing wind turbine towers using smaller particles may be effective at reducing similarity of the towers to water. Nevertheless, even for playback of our highest frequency source call (100-90 kHz) at our shallowest angle (40°), we found that the coarse texture consistently showed the most pronounced acoustic differences from smooth surfaces across all three response variables.

To confirm that the results in our study are equivalent to those of Greif and Siemers (2010), we played the 120-20 kHz synthetic FM sweep at a 40° angle of incidence toward our experimental surfaces. Visually comparing our spectrogram images to those obtained by Greif and Siemers (2010), we confirmed that our smooth unpainted and smooth painted surfaces contained only a single reflected echo and appeared similar to their smooth metal surface and water surfaces (Fig. 29). In contrast, our

textured surfaces consisted of multiple overlapping echoes and appeared similar to the their textured surfaces (Fig. 29).

One consideration we have not yet addressed is the degree to which our different textured surfaces might cause a wind turbine tower to resemble a resource that bats may be attracted to (e.g., a tree). While we have focused on whether bats may misperceive the smooth surfaces of wind turbine towers to be water, it has also been suggested that bats may be attracted to wind turbines because they perceive them to be tall trees (Cryan et al. 2014). In this study, we did not have a surface that was an actual section of a tree trunk; however, we did include a wood chip surface to represent an equivalent surface. Unexpectedly, this surface produced echoes that were more similar to water than the echoes produced by our coarse texture in nearly all experimental trials, and generally produced intensity, spectral, and temporal differences from smooth surfaces that were intermediate to those of the medium and fine texture. Despite this, echoes reflecting off of the wood chip surface often appeared qualitatively different from echoes reflecting off of the three sand-textured surfaces. These qualitative differences were likely due to reflecting surfaces in the wood chip texture that were relatively flat compared to the irregular shapes of sand texture particles. This result provides some indication that texturing wind turbine tower surfaces using sand-based texture particles will not transform them into a surface that bats perceive to be trees through echolocation.

There were potential limitations of our study that should be addressed. One limitation was that our speaker emitted each source call with constant directionality determined by frequency, whereas bats are able to adjust the directionality of their echolocation calls (Jakobsen et al. 2013, Kounitsky et al. 2015). This property is potentially important because we observed that the low directionality of low frequency source calls (e.g., 30-20 kHz sweep) reduced the acoustic differences between smooth and textured surfaces. Directionality was likely one of the reasons our findings suggest that low frequency bat species have less acoustic information available to them to differentiate smooth and textured

surfaces. Nevertheless, the three low frequency bat species among our study species are all known to be adapted to long-range target detection and forage in relatively open spaces with minimal clutter as would be expected for species with low call directionality (Simmons et al. 1978, Barclay 1986).

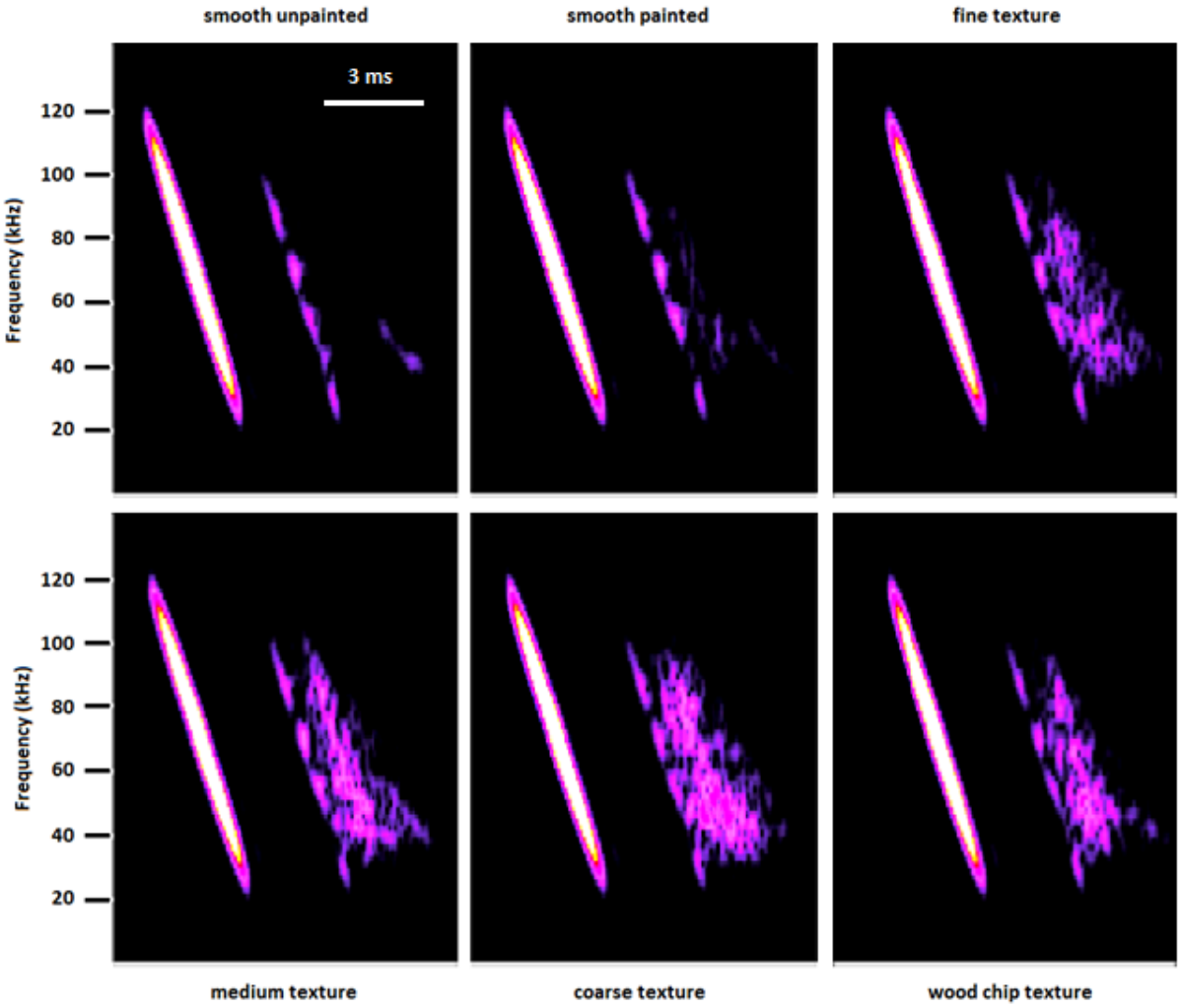

Figure 29. Spectrograms of echoes returning from playback of the 120-20 kHz FM sweep at a 40° angle of incidence, recreating the result obtained by Greif and Siemers (2010) for our experimental surfaces. The first signal in each panel is the outgoing source call; signals that follow are returning echoes. Lighter colors represent greater sound intensity. Smooth surfaces returned a single echo approximately 2.9 ms after the source call, indicating that the echo originated from the normal directly below the playback setup, whereas textured surfaces returned echoes that consisted of both the normal echo and multiple reflections from the textures with durations extending beyond 2.9 ms after the source call.

Another limitation is that we used only the strongest harmonic emitted by each species to generate our synthetic frequency sweeps. The reasoning behind this was that the relative intensities of the different harmonics are (1) not well-known for our study species, (2) may vary depending on the task the bat is attempting to perform, and (3) would add complexity to our analysis without necessarily adding to our findings. Yet, *in situ*, many bats use harmonics to improve ranging accuracy by increasing their call bandwidth, and to gather additional information about their environment (Fenton 2013, Mora et al. 2013). We note that it may be possible that low frequency bat species may use higher frequencies in the form of harmonics to investigate surface features, especially silver-haired bats which are known to emit multiharmonic search and approach calls (Barclay 1986). Nevertheless, we can approximate the ability of low frequency bat species to differentiate surface textures using higher frequency harmonics by examining the results of our FM sweeps at frequencies corresponding to these harmonics. Furthermore, as we observed measurable acoustic differences between smooth and textured surfaces at low frequencies without the inclusion of higher frequency harmonics, compensating for this limitation would likely not affect the overall results of our study.

As an additional point of interest, Siemers et al. (2001) proposed that some bat species selectively forage over calm water surfaces to take advantage of an acoustic mirror effect that makes prey conspicuous against a quiet background. Indeed, previous research suggests that bats prefer calm water for both drinking and foraging, which indicates that bats are attracted to water sources not only to drink, but also to forage (von Frenckell and Barclay 1987, Mackey and Barclay 1989, Adams and Simmons 2002). McAlexander (2013) suggested that a wind turbine tower surface might also function as an acoustic mirror and could potentially improve the bats' prey capture rates. Although it is unknown whether bats use the acoustic mirror effect to improve foraging efficiency at wind turbines, our study demonstrated that texturing wind turbine tower-equivalent surfaces can dramatically increase the amount of echo energy returning from bat echolocation calls at shallow angles. We speculate that

adding texture may reduce the acoustic mirror effect on a wind turbine tower surface and therefore reduce the ability of bats to forage efficiently at wind turbines (cf. Simmons et al. 1989, Rydell et al. 1999). In turn, if wind turbines do not provide foraging opportunities that are similar or greater than are available in the surrounding areas then bats should avoid foraging at wind turbines. Thus, it is possible that texturing wind turbine towers may reduce the attractiveness of wind turbines to bats in two ways: (1) reduce the acoustic similarity to water, and (2) create a less efficient foraging environment for bats.

CONCLUSION

Based on our findings, we recommend textures with large particle sizes for texturing of wind turbine tower surfaces as they are the most acoustically dissimilar to water and also provide the greatest level of clutter echo. Note that our recommendation is based on the assumption that other aspects of coarse textures are not disadvantageous. As our experiment cannot inform on the possibility that bats may be attracted to textured surfaces for reasons other than attraction to water (e.g., attraction to tree bark), we also recommend behavioral testing of textured surfaces incorporating large particle sizes, with bats *ex situ*. If these surfaces do not show attraction with captive bats, we recommend small-scale implementation at operating wind energy facilities to determine the effectiveness of texturing wind turbine towers as a means of reducing bat fatalities. If texturing wind turbine towers reduces the attractiveness of wind turbines to bats, then texturing new and existing wind turbine towers may prove to be a cost-effective means of reducing bat fatality rates while maximizing renewable energy generation.

APPENDIX A**:** Source calls used in the playback experiment.

Call ID	Species	Source Call	Duration (ms)	Wavelength Range (mm)
1	-	120-20 kHz FM sweep	3.0	2.9 – 17.2
2	-	30-20 kHz FM sweep	1.5	11.4 – 17.2
3	-	40-30 kHz FM sweep	1.5	8.6 – 11.4
4	-	50-40 kHz FM sweep	1.5	6.9 – 8.6
5	-	60-50 kHz FM sweep	1.5	5.7 – 6.9
6	-	70-60 kHz FM sweep	1.5	4.9 – 5.7
7	-	80-70 kHz FM sweep	1.5	4.3 – 4.9
8	-	90-80 kHz FM sweep	1.5	3.8 – 4.3
9	-	100-90 kHz FM sweep	1.5	3.4 – 3.8
10	Laci	41-23 kHz approach call	2.0	8.4 – 14.9
11	Laci	45-20 kHz terminal buzz	1.0	7.6 – 17.2
12	Tabr	45-28 kHz approach call	2.0	7.6 – 12.3
13	Tabr	45-23 kHz terminal buzz	1.0	7.6 – 14.9
14	Lano	48-28 kHz approach call	2.0	7.1 – 12.3
15	Lano	44-26 kHz terminal buzz	1.0	7.8 – 13.2
16	Nyhu	64-36 kHz approach call	2.0	5.4 – 9.5
17	Nyhu	59-33 kHz terminal buzz	1.0	5.8 – 10.4
18	Labo	76-41 kHz approach call	2.0	4.5 – 8.4
19	Labo	62-38 kHz terminal buzz	1.0	5.5 – 9.0
20	Pesu	62-43 kHz approach call	2.0	5.5 – 8.0
21	Pesu	61-39 kHz terminal buzz	1.0	5.6 – 8.8
22	Mylu	65-42 kHz terminal buzz	1.0	5.3 – 8.2
23	Myse	80-43 kHz terminal buzz	1.0	4.3 – 8.0

APPENDIX B: Presentation order of angles of incidence on each day.

	Day 1	Day 2	Day 3
1st Angle	20°	0°	40°
2nd Angle	40°	20°	0°
3rd Angle	0°	40°	20°

APPENDIX C: Example randomized Latin square experimental design.

Set 1	Set 2	Set 3	Set 4	Set 5	Set 6
1 Medium Texture	7 Coarse Texture	13 Fine Texture	19 Smooth Unpainted	25 Wood Chip	31 Smooth Painted
2 Coarse Texture	8 Smooth Painted	14 Smooth Unpainted	20 Medium Texture	26 Fine Texture	32 Wood Chip
3 Fine Texture	9 Wood Chip	15 Medium Texture	21 Smooth Painted	27 Coarse Texture	33 Smooth Unpainted
4 Smooth Unpainted	10 Fine Texture	16 Smooth Painted	22 Wood Chip	28 Medium Texture	34 Coarse Texture
5 Smooth Painted	11 Medium Texture	17 Wood Chip	23 Coarse Texture	29 Smooth Unpainted	35 Fine Texture
6 Wood Chip	12 Smooth Unpainted	18 Coarse Texture	24 Fine Texture	30 Smooth Painted	36 Medium Texture

APPENDIX D: Minimum amplitude thresholds for each angle-call combination in playback analysis.

Source Call	0° threshold (dB SPL)	20° threshold (dB SPL)	40° threshold (dB SPL)
120-20 kHz FM sweep	35.0	35.0	30.0
30-20 kHz FM sweep	40.0	40.0	35.0
40-30 kHz FM sweep	35.0	35.0	30.0
50-40 kHz FM sweep	35.0	35.0	30.0
60-50 kHz FM sweep	35.0	35.0	30.0
70-60 kHz FM sweep	35.0	30.0	25.0
80-70 kHz FM sweep	35.0	30.0	25.0
90-80 kHz FM sweep	35.0	25.0	25.0
100-90 kHz FM sweep	25.0	25.0	25.0
41-23 kHz approach call (Laci)	40.0	40.0	40.0
45-20 kHz terminal buzz (Laci)	40.0	40.0	35.0
45-28 kHz approach call (Tabr)	40.0	40.0	40.0
45-23 kHz terminal buzz (Tabr)	40.0	40.0	35.0
48-28 kHz approach call (Lano)	40.0	40.0	40.0
44-26 kHz terminal buzz (Lano)	40.0	40.0	35.0
64-36 kHz approach call (Nyhu)	40.0	40.0	35.0
59-33 kHz terminal buzz (Nyhu)	40.0	40.0	30.0
76-41 kHz approach call (Labo)	40.0	40.0	35.0
62-38 kHz terminal buzz (Labo)	40.0	40.0	30.0
62-43 kHz approach call (Pesu)	40.0	40.0	30.0
61-39 kHz terminal buzz (Pesu)	40.0	40.0	30.0
65-42 kHz terminal buzz (Mylu)	40.0	40.0	30.0
80-43 kHz terminal buzz (Myse)	35.0	30.0	25.0

APPENDIX E: Means and SEs (n = 3) maximum peak amplitude (dB SPL) for synthetic FM sweep echoes.

	0°		20°		40°	
	Mean	**SEM**	**Mean**	**SEM**	**Mean**	**SEM**
120—20 kHz						
Smooth Painted	**60.096**	0.732	**56.930**	0.998	**39.888**	0.331
Smooth Unpainted	**60.062**	0.668	**56.868**	1.042	**40.196**	0.323
Fine Texture	**60.233**	0.738	**57.028**	1.067	**45.368**	0.517
Medium Texture	**60.144**	0.717	**57.628**	1.042	**47.424**	0.082
Coarse Texture	**60.074**	0.912	**58.056**	0.314	**50.429**	0.446
Wood Chip Texture	**59.860**	0.923	**57.420**	0.575	**45.163**	0.731
30—20 kHz						
Smooth Painted	**68.879**	0.622	**69.808**	0.947	**65.520**	1.395
Smooth Unpainted	**68.782**	0.511	**69.728**	0.953	**65.750**	1.350
Fine Texture	**68.943**	0.591	**69.533**	1.022	**65.758**	1.198
Medium Texture	**69.180**	0.578	**69.776**	0.941	**65.696**	1.329
Coarse Texture	**68.840**	0.701	**69.851**	0.944	**65.691**	1.305
Wood Chip Texture	**68.815**	0.634	**69.672**	0.913	**65.681**	1.422
40—30 kHz						
Smooth Painted	**69.596**	1.040	**70.523**	0.370	**48.493**	2.250
Smooth Unpainted	**69.603**	0.874	**70.469**	0.390	**48.872**	2.289
Fine Texture	**69.743**	1.037	**70.555**	0.113	**50.313**	1.336
Medium Texture	**69.997**	0.978	**71.036**	0.154	**54.094**	0.782
Coarse Texture	**69.624**	1.129	**70.207**	1.073	**57.341**	0.412
Wood Chip Texture	**69.433**	0.997	**70.249**	0.670	**54.203**	0.408
50—40 kHz						
Smooth Painted	**71.746**	0.542	**66.573**	1.696	**42.011**	1.751
Smooth Unpainted	**71.640**	0.423	**67.228**	0.988	**41.035**	2.222
Fine Texture	**71.916**	0.556	**67.992**	0.379	**53.834**	1.011
Medium Texture	**71.676**	0.480	**66.664**	1.618	**56.483**	0.679
Coarse Texture	**71.565**	0.839	**68.193**	0.794	**60.175**	1.119
Wood Chip Texture	**71.481**	0.681	**68.498**	0.244	**56.038**	0.677
60—50 kHz						
Smooth Painted	**63.409**	1.100	**56.907**	2.352	**46.814**	0.942
Smooth Unpainted	**63.327**	1.100	**56.765**	2.439	**47.184**	0.888
Fine Texture	**63.437**	1.164	**57.794**	2.494	**49.869**	0.246
Medium Texture	**63.388**	1.099	**58.004**	1.409	**52.566**	0.247
Coarse Texture	**62.643**	1.710	**59.623**	1.699	**54.364**	0.767
Wood Chip Texture	**63.152**	1.223	**58.290**	1.633	**49.684**	0.309
70—60 kHz						
Smooth Painted	**57.953**	2.199	**52.195**	0.874	**37.385**	1.338
Smooth Unpainted	**58.188**	2.030	**52.472**	1.051	**37.242**	1.832
Fine Texture	**57.894**	2.207	**54.342**	0.626	**46.591**	0.541
Medium Texture	**58.865**	1.502	**53.621**	0.419	**47.201**	0.260
Coarse Texture	**57.626**	2.372	**55.347**	0.748	**48.703**	0.521
Wood Chip Texture	**57.757**	2.055	**53.296**	1.051	**45.393**	0.722
80—70 kHz						
Smooth Painted	**51.632**	4.229	**48.254**	1.734	**33.645**	2.488
Smooth Unpainted	**51.372**	4.948	**48.509**	1.975	**32.295**	3.231
Fine Texture	**51.346**	4.419	**51.087**	1.059	**45.035**	0.809
Medium Texture	**52.659**	4.053	**52.859**	1.031	**46.458**	0.745
Coarse Texture	**51.242**	4.207	**53.852**	1.825	**48.490**	0.383
Wood Chip Texture	**51.809**	3.635	**51.766**	0.065	**42.674**	0.141
90—80 kHz						
Smooth Painted	**51.649**	3.820	**42.052**	2.630	**41.051**	3.021
Smooth Unpainted	**52.259**	3.298	**40.547**	3.797	**40.819**	3.318
Fine Texture	**51.841**	3.521	**49.012**	0.709	**45.566**	0.357
Medium Texture	**51.185**	3.674	**50.219**	1.275	**47.191**	0.270
Coarse Texture	**50.687**	4.315	**52.466**	0.737	**46.997**	0.619
Wood Chip Texture	**52.443**	3.056	**48.285**	0.897	**43.449**	0.948
100—90 kHz						
Smooth Painted	**45.530**	5.296	**40.537**	0.822	**38.456**	2.119
Smooth Unpainted	**46.169**	4.409	**40.031**	0.764	**38.957**	1.974
Fine Texture	**45.688**	4.283	**44.344**	0.406	**41.220**	0.503
Medium Texture	**45.813**	3.873	**45.671**	0.655	**40.673**	1.469
Coarse Texture	**45.464**	4.606	**45.758**	0.655	**42.155**	0.623
Wood Chip Texture	**45.926**	4.847	**44.003**	1.166	**39.462**	1.155

APPENDIX F: Means and SEs (n = 3) mean Wiener entropy (a. u.) for synthetic FM sweep echoes.

	0°		20°		40°	
	Mean	**SEM**	**Mean**	**SEM**	**Mean**	**SEM**
120—20 kHz						
Smooth Painted	**0.340**	0.004	**0.344**	0.003	**0.505**	0.002
Smooth Unpainted	**0.339**	0.005	**0.339**	0.003	**0.468**	0.006
Fine Texture	**0.340**	0.004	**0.373**	0.007	**0.475**	0.003
Medium Texture	**0.341**	0.005	**0.378**	0.008	**0.466**	0.001
Coarse Texture	**0.341**	0.005	**0.375**	0.005	**0.447**	0.004
Wood Chip Texture	**0.340**	0.004	**0.373**	0.005	**0.473**	0.002
30—20 kHz						
Smooth Painted	**0.221**	0.002	**0.205**	0.002	**0.198**	<0.001
Smooth Unpainted	**0.222**	0.002	**0.205**	0.002	**0.197**	0.001
Fine Texture	**0.221**	0.002	**0.206**	0.003	**0.211**	0.004
Medium Texture	**0.220**	0.001	**0.208**	0.001	**0.220**	0.004
Coarse Texture	**0.223**	0.003	**0.221**	0.001	**0.221**	0.004
Wood Chip Texture	**0.222**	0.002	**0.209**	0.005	**0.213**	0.002
40—30 kHz						
Smooth Painted	**0.218**	0.002	**0.226**	0.002	**0.373**	0.018
Smooth Unpainted	**0.218**	0.002	**0.226**	0.002	**0.348**	0.017
Fine Texture	**0.219**	0.002	**0.236**	0.001	**0.343**	0.003
Medium Texture	**0.220**	0.002	**0.243**	0.007	**0.313**	0.010
Coarse Texture	**0.222**	0.001	**0.247**	0.007	**0.301**	0.009
Wood Chip Texture	**0.219**	0.002	**0.232**	0.003	**0.322**	0.003
50—40 kHz						
Smooth Painted	**0.213**	0.001	**0.244**	0.015	**0.434**	0.018
Smooth Unpainted	**0.213**	0.001	**0.233**	0.005	**0.411**	0.038
Fine Texture	**0.213**	0.001	**0.235**	0.003	**0.314**	0.003
Medium Texture	**0.213**	0.001	**0.246**	0.010	**0.286**	0.004
Coarse Texture	**0.215**	0.002	**0.236**	0.006	**0.273**	0.004
Wood Chip Texture	**0.214**	0.001	**0.232**	0.005	**0.304**	0.001
60—50 kHz						
Smooth Painted	**0.225**	0.001	**0.236**	0.005	**0.390**	0.009
Smooth Unpainted	**0.226**	0.002	**0.233**	0.004	**0.342**	0.011
Fine Texture	**0.226**	0.002	**0.249**	0.009	**0.311**	0.003
Medium Texture	**0.225**	0.001	**0.247**	0.006	**0.315**	0.006
Coarse Texture	**0.226**	0.002	**0.247**	0.003	**0.294**	0.007
Wood Chip Texture	**0.226**	0.001	**0.248**	0.007	**0.320**	0.012
70—60 kHz						
Smooth Painted	**0.231**	0.003	**0.291**	0.003	**0.551**	0.020
Smooth Unpainted	**0.231**	0.003	**0.289**	0.002	**0.510**	0.042
Fine Texture	**0.231**	0.003	**0.303**	0.003	**0.418**	0.009
Medium Texture	**0.229**	0.002	**0.306**	0.004	**0.400**	0.012
Coarse Texture	**0.234**	0.005	**0.304**	0.005	**0.403**	0.012
Wood Chip Texture	**0.232**	0.002	**0.303**	0.006	**0.438**	0.011
80—70 kHz						
Smooth Painted	**0.264**	0.023	**0.325**	0.015	**0.599**	0.044
Smooth Unpainted	**0.273**	0.035	**0.317**	0.013	**0.608**	0.064
Fine Texture	**0.268**	0.024	**0.321**	0.006	**0.432**	0.017
Medium Texture	**0.262**	0.023	**0.306**	0.008	**0.432**	0.009
Coarse Texture	**0.269**	0.023	**0.301**	0.008	**0.394**	0.015
Wood Chip Texture	**0.261**	0.019	**0.301**	0.002	**0.463**	0.009
90—80 kHz						
Smooth Painted	**0.259**	0.023	**0.438**	0.037	**0.495**	0.020
Smooth Unpainted	**0.255**	0.017	**0.461**	0.059	**0.482**	0.038
Fine Texture	**0.257**	0.020	**0.381**	0.008	**0.404**	0.013
Medium Texture	**0.263**	0.020	**0.374**	0.015	**0.387**	0.015
Coarse Texture	**0.272**	0.028	**0.361**	0.004	**0.389**	0.013
Wood Chip Texture	**0.252**	0.017	**0.384**	0.011	**0.426**	0.024
100—90 kHz						
Smooth Painted	**0.407**	0.065	**0.454**	0.006	**0.536**	0.027
Smooth Unpainted	**0.403**	0.056	**0.458**	0.007	**0.481**	0.038
Fine Texture	**0.404**	0.053	**0.426**	0.008	**0.465**	0.014
Medium Texture	**0.399**	0.040	**0.415**	0.013	**0.461**	0.023
Coarse Texture	**0.410**	0.053	**0.396**	0.009	**0.469**	0.020
Wood Chip Texture	**0.405**	0.062	**0.416**	0.010	**0.513**	0.026

APPENDIX G: Means and SEs (n = 3) temporal waveform variation (a. u.) for synthetic FM sweep echoes.

	0°		20°		40°	
	Mean	**SEM**	**Mean**	**SEM**	**Mean**	**SEM**
120—20 kHz						
Painted – Painted	1.049	0.198	0.883	0.077	13.901	2.448
Painted – Unpainted	1.298	0.479	1.215	0.274	15.571	2.020
Painted – Fine	1.552	0.210	5.074	0.813	156.318	17.900
Painted – Medium	2.089	0.473	8.395	0.707	158.260	13.797
Painted – Coarse[+]	**2.188**	0.641	**26.171**	0.840	**200.727**	12.048
Painted – Wood Chip	2.071	0.291	9.879	1.665	165.259	7.589
30—20 kHz						
Painted – Painted	0.700	0.244	0.585	0.090	0.474	0.071
Painted – Unpainted	0.689	0.073	0.603	0.090	0.456	0.069
Painted – Fine	0.682	0.120	1.137	0.164	2.077	0.361
Painted – Medium	0.738	0.068	2.102	0.410	3.744	1.178
Painted – Coarse[+]	0.611	0.079	**4.507**	1.068	**12.245**	0.991
Painted – Wood Chip[+]	**0.777**	0.302	2.948	0.854	6.956	1.981
40—30 kHz						
Painted – Painted	0.943	0.376	0.405	0.137	13.878	6.383
Painted – Unpainted	0.752	0.112	0.264	0.036	9.590	3.143
Painted – Fine	0.608	0.129	1.672	0.122	89.389	27.678
Painted – Medium[+]	0.902	0.153	3.647	0.517	**142.330**	9.305
Painted – Coarse[+]	**1.256**	0.299	**15.900**	4.133	123.031	21.209
Painted – Wood Chip	0.954	0.297	4.658	0.652	114.035	22.321
50—40 kHz						
Painted – Painted	0.259	0.082	0.700	0.123	-	-
Painted – Unpainted	0.368	0.011	0.370	0.041	-	-
Painted – Fine	0.462	0.104	7.067	2.443	-	-
Painted – Medium	0.406	0.033	8.708	0.199	-	-
Painted – Coarse[+]	**0.776**	0.142	**38.668**	10.169	-	-
Painted – Wood Chip	0.426	0.050	14.418	3.321	-	-
60—50 kHz						
Painted – Painted	0.180	0.043	2.809	1.373	6.039	0.874
Painted – Unpainted	0.469	0.024	1.379	0.451	5.550	0.947
Painted – Fine	0.428	0.204	15.532	5.687	188.832	29.513
Painted – Medium	0.673	0.190	27.384	8.836	205.381	9.032
Painted – Coarse[+]	**0.986**	0.133	**60.248**	18.132	**229.271**	22.518
Painted – Wood Chip	0.871	0.211	20.806	5.816	166.206	2.320
70—60 kHz						
Painted – Painted	0.960	0.281	3.990	1.856	26.251	8.686
Painted – Unpainted	0.354	0.189	2.376	0.671	33.087	9.072
Painted – Fine	0.505	0.057	21.117	8.093	173.250	25.012
Painted – Medium	1.308	0.584	38.820	11.503	181.809	29.163
Painted – Coarse[+]	**1.877**	0.651	**70.248**	8.660	**181.824**	25.853
Painted – Wood Chip	1.273	0.556	26.059	5.558	155.555	14.653
80—70 kHz						
Painted – Painted	2.252	1.156	14.155	7.645	-	-
Painted – Unpainted	15.394	14.086	7.955	3.608	-	-
Painted – Fine	5.156	2.949	48.674	7.056	-	-
Painted – Medium[+]	**20.945**	18.977	65.906	12.386	-	-
Painted – Coarse[+]	8.879	5.471	**75.734**	3.819	-	-
Painted – Wood Chip	5.172	2.552	53.268	10.621	-	-
90—80 kHz						
Painted – Painted	0.960	0.281	41.236	14.887	52.134	22.411
Painted – Unpainted	1.055	0.282	30.712	13.911	23.725	17.366
Painted – Fine	2.029	1.147	82.566	21.526	158.143	9.470
Painted – Medium	4.060	2.201	81.360	18.375	178.280	26.539
Painted – Coarse[+]	**4.719**	1.881	**86.231**	12.079	**182.462**	11.633
Painted – Wood Chip	1.534	0.626	64.812	10.972	130.718	14.796
100—90 kHz						
Painted – Painted	6.875	5.976	25.864	4.221	15.779	9.582
Painted – Unpainted	17.078	16.275	18.518	5.375	18.286	7.703
Painted – Fine	18.405	16.316	77.825	12.819	132.416	35.040
Painted – Medium[+]	18.027	14.942	**93.494**	16.127	126.701	26.350
Painted – Coarse[+]	**22.398**	20.308	84.489	15.887	**138.827**	16.350
Painted – Wood Chip	13.815	12.285	68.583	15.109	74.274	24.695

[+] surface comparison identified as having the highest temporal waveform variation for at least one angle

APPENDIX H: Means and SEs (n = 3) maximum peak amplitude (dB SPL) for synthetic bat call echoes.

	0°		20°		40°	
	Mean	**SEM**	**Mean**	**SEM**	**Mean**	**SEM**
Synthetic Approach Calls						
Laci (41 – 23 kHz)						
Smooth Painted	**69.779**	0.630	**72.599**	0.823	**67.525**	1.543
Smooth Unpainted	**69.687**	0.523	**72.483**	0.871	**67.740**	1.508
Fine Texture	**69.828**	0.586	**72.290**	0.964	**67.736**	1.371
Medium Texture	**70.051**	0.594	**72.492**	0.845	**67.716**	1.481
Coarse Texture	**69.774**	0.741	**72.535**	0.797	**67.788**	1.378
Wood Chip Texture	**69.731**	0.645	**72.387**	0.822	**67.658**	1.533
Tabr (45 – 28 kHz)						
Smooth Painted	**70.386**	0.613	**65.115**	1.564	**62.687**	0.832
Smooth Unpainted	**70.292**	0.478	**64.978**	1.608	**62.821**	0.801
Fine Texture	**70.544**	0.587	**65.027**	1.694	**62.811**	0.966
Medium Texture	**70.749**	0.565	**65.746**	1.262	**62.802**	0.943
Coarse Texture	**70.336**	0.698	**66.440**	1.058	**62.672**	0.744
Wood Chip Texture	**70.264**	0.629	**64.566**	0.912	**62.755**	0.997
Lano (48 – 28 kHz)						
Smooth Painted	**70.171**	0.639	**65.249**	1.431	**62.403**	0.841
Smooth Unpainted	**70.084**	0.506	**65.105**	1.468	**62.540**	0.806
Fine Texture	**70.320**	0.611	**65.142**	1.519	**62.519**	0.984
Medium Texture	**70.546**	0.598	**65.893**	1.168	**62.501**	0.933
Coarse Texture	**70.121**	0.707	**66.649**	0.895	**62.351**	0.743
Wood Chip Texture	**70.057**	0.655	**64.765**	0.825	**62.439**	1.010
Nyhu (64 – 36 kHz)						
Smooth Painted	**70.387**	1.255	**71.211**	0.690	**39.941**	1.180
Smooth Unpainted	**70.394**	1.106	**71.169**	0.626	**41.375**	1.034
Fine Texture	**70.536**	1.286	**70.959**	0.705	**51.220**	1.410
Medium Texture	**70.772**	1.186	**71.281**	0.876	**54.799**	1.115
Coarse Texture	**70.414**	1.286	**70.534**	0.680	**60.539**	0.483
Wood Chip Texture	**70.189**	1.253	**71.650**	0.424	**54.476**	0.083
Labo (76 – 41 kHz)						
Smooth Painted	**71.731**	1.047	**66.552**	0.702	**42.495**	2.047
Smooth Unpainted	**71.786**	0.909	**66.428**	0.678	**42.340**	2.230
Fine Texture	**71.937**	1.065	**66.773**	0.459	**54.404**	0.881
Medium Texture	**72.053**	1.006	**67.014**	0.155	**57.022**	0.652
Coarse Texture	**71.564**	1.335	**67.932**	0.459	**60.694**	0.582
Wood Chip Texture	**71.450**	1.253	**68.170**	0.129	**54.996**	0.474
Pesu (62 – 43 kHz)						
Smooth Painted	**72.959**	0.663	**68.999**	0.611	**43.675**	1.882
Smooth Unpainted	**72.885**	0.541	**68.874**	0.594	**42.444**	2.957
Fine Texture	**73.157**	0.675	**69.142**	0.454	**54.770**	1.173
Medium Texture	**72.995**	0.616	**69.210**	0.080	**58.422**	0.154
Coarse Texture	**72.811**	0.976	**70.175**	0.800	**61.764**	0.859
Wood Chip Texture	**72.700**	0.836	**70.279**	0.102	**56.635**	0.846
Synthetic Terminal Buzz Calls						
Laci (45 – 20 kHz)						
Smooth Painted	**64.533**	0.878	**64.720**	0.342	**54.797**	0.862
Smooth Unpainted	**64.519**	0.701	**64.641**	0.362	**54.937**	0.861
Fine Texture	**64.650**	0.857	**64.694**	0.146	**54.936**	0.997
Medium Texture	**64.901**	0.835	**65.344**	0.156	**54.645**	0.982
Coarse Texture	**64.487**	0.915	**65.218**	0.734	**54.952**	0.974
Wood Chip Texture	**64.408**	0.787	**64.697**	0.463	**54.810**	0.993
Tabr (45 – 23 kHz)						
Smooth Painted	**65.244**	0.956	**66.049**	0.170	**52.418**	1.420
Smooth Unpainted	**65.235**	0.784	**65.976**	0.196	**52.498**	1.393
Fine Texture	**65.375**	0.951	**65.984**	0.067	**52.451**	1.542
Medium Texture	**65.620**	0.899	**66.619**	0.015	**52.457**	1.196
Coarse Texture	**65.239**	1.028	**66.135**	0.780	**54.444**	0.669
Wood Chip Texture	**65.112**	0.877	**66.048**	0.342	**53.040**	0.997

APPENDIX H continued

	0°		20°		40°	
	Mean	**SEM**	**Mean**	**SEM**	**Mean**	**SEM**
Lano (44 – 26 kHz)						
Smooth Painted	**65.962**	1.048	**67.181**	0.092	**50.097**	1.880
Smooth Unpainted	**65.960**	0.881	**67.111**	0.113	**50.237**	1.844
Fine Texture	**66.103**	1.043	**67.104**	0.102	**50.076**	1.942
Medium Texture	**66.350**	0.979	**67.684**	0.140	**51.704**	0.883
Coarse Texture	**65.993**	1.127	**67.007**	0.783	**54.713**	0.478
Wood Chip Texture	**65.829**	0.999	**67.207**	0.240	**51.952**	0.727
Nyhu (59 – 33 kHz)						
Smooth Painted	**66.514**	0.547	**62.954**	0.421	**38.220**	1.167
Smooth Unpainted	**66.399**	0.424	**62.842**	0.416	**38.531**	1.067
Fine Texture	**66.659**	0.555	**62.972**	0.407	**50.774**	0.396
Medium Texture	**66.441**	0.488	**63.769**	0.585	**51.761**	0.453
Coarse Texture	**66.403**	0.803	**64.173**	0.233	**55.832**	0.802
Wood Chip Texture	**66.243**	0.682	**63.985**	0.248	**50.961**	0.717
Labo (62 – 38 kHz)						
Smooth Painted	**65.105**	0.858	**61.495**	1.325	**39.467**	0.263
Smooth Unpainted	**65.084**	0.768	**61.415**	1.376	**39.456**	0.298
Fine Texture	**65.265**	0.843	**61.596**	1.318	**49.840**	0.817
Medium Texture	**65.195**	0.793	**62.224**	1.349	**51.113**	0.495
Coarse Texture	**65.108**	0.974	**62.550**	0.380	**54.195**	0.866
Wood Chip Texture	**64.882**	1.016	**61.656**	1.085	**49.546**	0.848
Pesu (61 – 39 kHz)						
Smooth Painted	**65.416**	0.893	**61.728**	1.413	**39.695**	0.112
Smooth Unpainted	**65.406**	0.802	**61.642**	1.466	**39.683**	0.073
Fine Texture	**65.578**	0.879	**61.833**	1.418	**50.106**	0.824
Medium Texture	**65.524**	0.822	**62.404**	1.429	**51.463**	0.540
Coarse Texture	**65.421**	1.014	**62.830**	0.418	**54.465**	0.834
Wood Chip Texture	**65.221**	1.042	**61.824**	1.210	**49.793**	0.862
Mylu (65 – 42 kHz)						
Smooth Painted	**62.665**	1.088	**58.120**	1.713	**41.638**	0.909
Smooth Unpainted	**62.695**	1.011	**58.134**	1.738	**41.972**	0.842
Fine Texture	**62.761**	1.111	**58.502**	1.828	**47.723**	0.220
Medium Texture	**62.787**	1.002	**58.512**	1.739	**50.640**	0.286
Coarse Texture	**62.451**	1.399	**59.606**	1.195	**52.924**	0.626
Wood Chip Texture	**62.551**	1.219	**58.569**	1.513	**47.179**	0.637
Myse (80 – 43 kHz)						
Smooth Painted	**54.155**	1.048	**48.611**	1.689	**37.204**	0.920
Smooth Unpainted	**54.035**	1.068	**48.516**	1.727	**37.485**	0.948
Fine Texture	**54.211**	1.092	**49.744**	1.833	**41.227**	0.676
Medium Texture	**54.069**	1.055	**50.003**	1.418	**44.145**	0.637
Coarse Texture	**53.709**	1.582	**51.967**	1.409	**45.609**	0.716
Wood Chip Texture	**54.053**	1.197	**50.209**	1.402	**40.976**	0.384

APPENDIX I: Means and SEs (n = 3) mean Wiener entropy (a. u.) for synthetic bat call echoes.

	0°		20°		40°	
	Mean	**SEM**	**Mean**	**SEM**	**Mean**	**SEM**
Synthetic Approach Calls						
Laci (41 – 23 kHz)						
Smooth Painted	**0.188**	0.001	**0.198**	0.001	**0.191**	0.001
Smooth Unpainted	**0.189**	0.001	**0.199**	<0.001	**0.189**	0.001
Fine Texture	**0.188**	<0.001	**0.200**	0.001	**0.207**	0.005
Medium Texture	**0.188**	<0.001	**0.204**	0.001	**0.212**	0.004
Coarse Texture	**0.189**	0.001	**0.217**	0.005	**0.218**	0.006
Wood Chip Texture	**0.189**	0.001	**0.203**	0.002	**0.208**	0.003
Tabr (45 – 28 kHz)						
Smooth Painted	**0.186**	0.001	**0.197**	0.009	**0.187**	0.002
Smooth Unpainted	**0.186**	0.001	**0.195**	0.008	**0.184**	0.002
Fine Texture	**0.186**	0.001	**0.206**	0.008	**0.223**	0.003
Medium Texture	**0.186**	<0.001	**0.215**	0.005	**0.220**	0.005
Coarse Texture	**0.188**	<0.001	**0.212**	0.001	**0.217**	0.002
Wood Chip Texture	**0.187**	0.001	**0.216**	0.004	**0.221**	0.003
Lano (48 – 28 kHz)						
Smooth Painted	**0.192**	<0.001	**0.201**	0.008	**0.190**	0.001
Smooth Unpainted	**0.192**	<0.001	**0.200**	0.007	**0.186**	0.001
Fine Texture	**0.193**	<0.001	**0.212**	0.008	**0.225**	0.007
Medium Texture	**0.192**	<0.001	**0.222**	0.004	**0.225**	0.004
Coarse Texture	**0.194**	<0.001	**0.220**	0.001	**0.224**	0.004
Wood Chip Texture	**0.193**	<0.001	**0.221**	0.005	**0.226**	0.003
Nyhu (64 – 36 kHz)						
Smooth Painted	**0.204**	0.001	**0.205**	0.001	**0.391**	0.017
Smooth Unpainted	**0.204**	<0.001	**0.205**	0.002	**0.363**	0.015
Fine Texture	**0.204**	<0.001	**0.210**	0.001	**0.315**	0.004
Medium Texture	**0.204**	<0.001	**0.212**	0.003	**0.288**	0.005
Coarse Texture	**0.205**	0.001	**0.218**	0.004	**0.267**	0.003
Wood Chip Texture	**0.204**	0.001	**0.216**	0.002	**0.302**	0.002
Labo (76 – 41 kHz)						
Smooth Painted	**0.207**	<0.001	**0.221**	0.005	**0.382**	0.021
Smooth Unpainted	**0.207**	0.001	**0.216**	0.004	**0.353**	0.024
Fine Texture	**0.207**	0.001	**0.227**	0.003	**0.301**	0.002
Medium Texture	**0.208**	<0.001	**0.223**	0.003	**0.277**	0.001
Coarse Texture	**0.210**	0.001	**0.223**	0.002	**0.259**	0.007
Wood Chip Texture	**0.208**	0.001	**0.220**	0.003	**0.293**	0.006
Pesu (62 – 43 kHz)						
Smooth Painted	**0.186**	<0.001	**0.190**	0.003	**0.406**	0.018
Smooth Unpainted	**0.186**	<0.001	**0.190**	0.004	**0.394**	0.038
Fine Texture	**0.186**	<0.001	**0.196**	0.004	**0.301**	0.003
Medium Texture	**0.186**	<0.001	**0.200**	0.004	**0.273**	0.002
Coarse Texture	**0.188**	<0.001	**0.194**	0.002	**0.261**	0.001
Wood Chip Texture	**0.186**	<0.001	**0.194**	0.001	**0.297**	0.005
Synthetic Terminal Buzz Calls						
Laci (45 – 20 kHz)						
Smooth Painted	**0.265**	0.001	**0.269**	0.001	**0.295**	0.003
Smooth Unpainted	**0.265**	0.001	**0.269**	0.002	**0.290**	0.003
Fine Texture	**0.266**	0.001	**0.275**	0.001	**0.332**	0.004
Medium Texture	**0.267**	<0.001	**0.283**	0.002	**0.319**	0.004
Coarse Texture	**0.269**	0.001	**0.283**	0.003	**0.313**	0.002
Wood Chip Texture	**0.266**	0.001	**0.282**	0.001	**0.326**	0.004
Tabr (45 – 23 kHz)						
Smooth Painted	**0.260**	<0.001	**0.262**	0.003	**0.299**	0.003
Smooth Unpainted	**0.260**	<0.001	**0.262**	0.002	**0.286**	0.005
Fine Texture	**0.260**	<0.001	**0.266**	0.003	**0.331**	0.005
Medium Texture	**0.260**	0.001	**0.273**	0.001	**0.319**	0.002
Coarse Texture	**0.262**	<0.001	**0.270**	0.003	**0.309**	0.003
Wood Chip Texture	**0.259**	0.001	**0.269**	0.003	**0.320**	0.004

APPENDIX I Continued

	0°		20°		40°	
	Mean	**SEM**	**Mean**	**SEM**	**Mean**	**SEM**
Lano (44 – 26 kHz)						
Smooth Painted	**0.247**	0.001	**0.247**	0.002	**0.304**	0.006
Smooth Unpainted	**0.248**	0.001	**0.248**	0.001	**0.291**	0.008
Fine Texture	**0.248**	0.001	**0.251**	0.002	**0.330**	0.004
Medium Texture	**0.249**	0.001	**0.255**	0.001	**0.312**	0.002
Coarse Texture	**0.250**	0.001	**0.253**	0.003	**0.299**	0.003
Wood Chip Texture	**0.248**	0.001	**0.251**	0.002	**0.314**	0.003
Nyhu (59 – 33 kHz)						
Smooth Painted	**0.267**	0.001	**0.267**	0.003	**0.466**	0.012
Smooth Unpainted	**0.267**	0.001	**0.267**	0.003	**0.438**	0.014
Fine Texture	**0.267**	0.001	**0.272**	0.002	**0.381**	0.004
Medium Texture	**0.267**	0.001	**0.274**	0.003	**0.349**	0.003
Coarse Texture	**0.268**	0.001	**0.271**	0.002	**0.329**	0.005
Wood Chip Texture	**0.268**	0.001	**0.270**	<0.001	**0.364**	0.001
Labo (62 – 38 kHz)						
Smooth Painted	**0.262**	<0.001	**0.257**	0.004	**0.442**	0.012
Smooth Unpainted	**0.263**	<0.001	**0.256**	0.004	**0.417**	0.006
Fine Texture	**0.263**	0.001	**0.267**	0.002	**0.364**	0.003
Medium Texture	**0.263**	<0.001	**0.267**	0.004	**0.355**	0.007
Coarse Texture	**0.263**	<0.001	**0.266**	0.003	**0.337**	0.003
Wood Chip Texture	**0.262**	<0.001	**0.265**	0.002	**0.353**	0.003
Pesu (61 – 39 kHz)						
Smooth Painted	**0.256**	<0.001	**0.252**	0.003	**0.439**	0.011
Smooth Unpainted	**0.256**	<0.001	**0.250**	0.003	**0.414**	0.007
Fine Texture	**0.257**	0.001	**0.260**	0.002	**0.358**	0.003
Medium Texture	**0.256**	<0.001	**0.261**	0.004	**0.350**	0.008
Coarse Texture	**0.256**	<0.001	**0.262**	0.003	**0.332**	0.003
Wood Chip Texture	**0.255**	<0.001	**0.259**	0.003	**0.348**	0.003
Mylu (65 – 42 kHz)						
Smooth Painted	**0.258**	0.003	**0.260**	0.003	**0.421**	0.009
Smooth Unpainted	**0.257**	0.003	**0.260**	0.004	**0.389**	0.002
Fine Texture	**0.258**	0.004	**0.272**	0.008	**0.364**	0.003
Medium Texture	**0.258**	0.003	**0.273**	0.005	**0.361**	0.009
Coarse Texture	**0.258**	0.003	**0.272**	0.003	**0.344**	0.005
Wood Chip Texture	**0.258**	0.003	**0.271**	0.004	**0.361**	0.005
Myse (80 – 43 kHz)						
Smooth Painted	**0.328**	0.003	**0.374**	0.004	**0.544**	0.009
Smooth Unpainted	**0.327**	0.002	**0.367**	0.003	**0.509**	0.005
Fine Texture	**0.328**	0.003	**0.394**	0.013	**0.475**	0.002
Medium Texture	**0.328**	0.002	**0.389**	0.007	**0.472**	0.004
Coarse Texture	**0.329**	0.003	**0.389**	0.007	**0.464**	0.003
Wood Chip Texture	**0.328**	0.003	**0.389**	0.008	**0.484**	0.006

APPENDIX J: Means and SEs (n = 3) temporal waveform variation (a. u.) for synthetic bat call echoes.

	0°		20°		40°	
	Mean	**SEM**	**Mean**	**SEM**	**Mean**	**SEM**
Synthetic Approach Calls						
Laci (41 – 23 kHz)						
Painted – Painted	0.884	0.122	0.581	0.038	0.583	0.120
Painted – Unpainted	0.768	0.078	0.890	0.109	0.574	0.061
Painted – Fine	0.823	0.197	1.150	0.077	2.061	0.235
Painted – Medium	0.771	0.083	2.037	0.342	3.598	1.173
Painted – Coarse^{+}	**0.968**	0.065	**4.034**	1.154	**10.895**	1.332
Painted – Wood Chip	0.761	0.250	2.773	0.825	6.935	2.016
Tabr (45 – 28 kHz)						
Painted – Painted	0.731	0.149	2.014	1.252	0.834	0.083
Painted – Unpainted	0.597	0.153	1.330	0.565	0.673	0.089
Painted – Fine	0.858	0.205	6.147	0.677	9.120	3.450
Painted – Medium	0.880	0.175	12.102	3.446	26.905	7.369
Painted – Coarse^{+}	**1.097**	0.217	**30.684**	9.632	**86.815**	14.311
Painted – Wood Chip	0.944	0.240	22.160	1.282	37.274	11.304
Lano (48 – 28 kHz)						
Painted – Painted	0.620	0.076	1.572	0.787	0.982	0.197
Painted – Unpainted	0.471	0.119	1.238	0.493	0.774	0.147
Painted – Fine	0.539	0.199	5.300	0.272	10.119	4.179
Painted – Medium	0.675	0.049	10.892	2.310	28.483	7.833
Painted – Coarse^{+}	**0.982**	0.023	**28.383**	8.613	**87.712**	14.602
Painted – Wood Chip	0.895	0.167	20.248	3.146	37.242	10.990
Nyhu (64 – 36 kHz)						
Painted – Painted	0.767	0.207	0.770	0.079	51.090	6.106
Painted – Unpainted	0.469	0.067	0.598	0.043	71.651	13.145
Painted – Fine	0.656	0.070	3.314	0.379	127.180	11.349
Painted – Medium	0.969	0.043	7.225	0.605	125.747	9.251
Painted – Coarse^{+}	**1.447**	0.423	**19.530**	1.544	138.213	8.246
Painted – Wood Chip^{+}	1.150	0.015	8.955	2.155	**147.649**	1.140
Labo (76 – 41 kHz)						
Painted – Painted	0.465	0.039	0.980	0.353	50.679	15.473
Painted – Unpainted	0.447	0.089	0.946	0.383	67.753	14.706
Painted – Fine	0.432	0.062	6.270	1.674	153.550	19.236
Painted – Medium	0.748	0.098	15.856	1.691	161.075	4.011
Painted – Coarse^{+}	0.948	0.046	**39.173**	4.745	**168.322**	13.545
Painted – Wood Chip^{+}	**0.982**	0.074	21.096	7.741	155.537	8.319
Pesu (62 – 43 kHz)						
Painted – Painted	1.016	0.350	1.279	0.395	74.109	23.878
Painted – Unpainted	0.888	0.142	0.638	0.149	68.102	21.310
Painted – Fine	0.506	0.096	10.616	3.707	144.599	18.190
Painted – Medium	0.919	0.109	14.586	0.512	149.493	7.904
Painted – Coarse^{+}	**1.088**	0.183	**47.702**	7.272	**165.081**	28.527
Painted – Wood Chip	1.011	0.163	18.349	3.808	161.101	11.669
Synthetic Terminal Buzz Calls						
Laci (45 – 20 kHz)						
Painted – Painted	0.297	0.069	0.380	0.167	0.524	0.027
Painted – Unpainted	0.261	0.046	0.328	0.076	0.503	0.091
Painted – Fine	0.502	0.154	0.836	0.053	9.470	3.610
Painted – Medium	0.538	0.204	1.372	0.252	26.670	3.993
Painted – Coarse^{+}	**0.826**	0.056	**6.581**	4.155	**74.074**	13.755
Painted – Wood Chip	0.386	0.118	2.522	1.076	20.820	5.009
Tabr (45 – 23 kHz)						
Painted – Painted	0.269	0.046	0.356	0.150	0.818	0.078
Painted – Unpainted	0.256	0.043	0.297	0.065	0.777	0.140
Painted – Fine	0.243	0.041	0.976	0.044	22.494	9.442
Painted – Medium	0.339	0.053	1.702	0.101	61.353	12.919
Painted – Coarse^{+}	**0.662**	0.215	**9.202**	2.425	**128.899**	30.643
Painted – Wood Chip	0.470	0.151	3.031	0.433	40.420	12.027

APPENDIX J Continued

	0°		20°		40°	
	Mean	**SEM**	**Mean**	**SEM**	**Mean**	**SEM**
Lano (44 – 26 kHz)						
Painted – Painted	0.486	0.147	0.368	0.145	1.757	0.389
Painted – Unpainted	0.365	0.112	0.268	0.070	1.779	0.462
Painted – Fine	0.357	0.076	1.089	0.103	48.561	19.836
Painted – Medium	0.526	0.132	2.091	0.152	107.913	21.954
Painted – Coarse[+]	**1.275**	0.510	**10.038**	2.002	**149.689**	25.196
Painted – Wood Chip	0.682	0.151	3.053	0.377	75.099	23.093
Nyhu (59 – 33 kHz)						
Painted – Painted	0.248	0.114	0.363	0.169	31.260	4.492
Painted – Unpainted	0.372	0.121	0.283	0.069	50.669	10.443
Painted – Fine	0.227	0.045	2.705	0.932	139.824	9.691
Painted – Medium	0.414	0.080	4.937	0.229	137.130	4.224
Painted – Coarse[+]	**0.769**	0.133	**20.192**	3.798	**161.719**	5.035
Painted – Wood Chip	0.465	0.047	8.998	1.553	148.646	7.061
Labo (62 – 38 kHz)						
Painted – Painted	0.313	0.100	0.433	0.168	20.709	1.432
Painted – Unpainted	0.487	0.084	0.372	0.101	31.640	3.588
Painted – Fine	0.336	0.107	3.401	0.830	136.414	9.809
Painted – Medium	0.400	0.052	7.378	1.665	135.859	12.781
Painted – Coarse[+]	**0.780**	0.225	**21.357**	0.583	**180.794**	10.947
Painted – Wood Chip	0.520	0.137	8.831	3.902	143.334	12.180
Pesu (61 – 39 kHz)						
Painted – Painted	0.336	0.080	0.399	0.141	22.989	2.019
Painted – Unpainted	0.249	0.060	0.341	0.093	34.007	3.967
Painted – Fine	0.335	0.038	3.483	0.757	139.959	7.815
Painted – Medium	0.455	0.218	7.959	1.844	140.717	12.624
Painted – Coarse[+]	**0.723**	0.217	**21.626**	1.170	**185.934**	10.436
Painted – Wood Chip	0.372	0.085	8.809	4.082	150.181	12.083
Mylu (65 – 42 kHz)						
Painted – Painted	0.719	0.172	0.902	0.349	8.689	0.897
Painted – Unpainted	0.734	0.042	0.907	0.283	12.973	1.879
Painted – Fine	0.783	0.265	4.438	0.682	133.749	5.615
Painted – Medium	0.800	0.299	12.043	3.585	130.826	10.345
Painted – Coarse[+]	**0.853**	0.240	**28.252**	7.438	**171.853**	3.691
Painted – Wood Chip	0.727	0.150	9.347	2.506	147.152	7.853
Myse (80 – 43 kHz)						
Painted – Painted	0.866	0.374	1.556	0.238	8.057	0.727
Painted – Unpainted	0.669	0.265	1.379	0.206	8.892	0.636
Painted – Fine	0.941	0.131	7.357	1.755	141.299	6.113
Painted – Medium[+]	**1.927**	0.480	15.830	5.055	143.818	7.367
Painted – Coarse[+]	1.791	0.206	**38.012**	12.033	**183.203**	5.232
Painted – Wood Chip	1.248	0.299	12.673	3.945	139.149	11.329

[+] **surface comparison identified as having the highest temporal waveform variation for at least one angle**

REFERENCES

Adams, R. A. and J. A. Simmons. 2002. Directionality of drinking passes by bats at water holes: is there cooperation? Acta Chiropterologica **4**(2): 195-199.

Ahlén, I., H. J. Baagøe and L. Bach. 2009. Behavior of Scandinavian bats during migration and foraging at sea. Journal of Mammalogy **90**(6): 1318-1323.

Arias-Coyotl, E., K. E. Stoner and A. Casas. 2006. Effectiveness of bats as pollinators of *Stenocereus stellatus* (Cactaceae) in wild, managed in situ, and cultivated populations in La Mixteca Baja, central Mexico. American Journal of Botany **93**(11): 1675-1683.

Arnett, E. B., and E. F. Baerwald. 2013. Impacts of wind energy development on bats: implications for conservation. Pages 435-456 in R. A. Adams and S. C. Pedersen, editors. Bat Evolution, Ecology, and Conservation. Springer Science Press, New York, NY.

Arnett, E. B., W. K. Brown, W. P. Erickson, J. K. Fiedler, B. L. Hamilton, T. H. Henry, A. Jain, G. D. Johnson, J. Kerns, R. R. Koford, C. P. Nicholson, T. J. O'Connell, M. D. Piorkowski and R. D. Tankersley. 2008. Patterns of bat fatalities at wind energy facilities in North America. Journal of Wildlife Management **72**(1): 61-78.

Aytekin, M., B. Mao and C. F. Moss. 2010. Spatial perception and adaptive sonar behavior. Journal of the Acoustical Society of America **128**(6): 3788-3798.

Baerwald, E. F. and R. M. R. Barclay. 2011. Patterns of activity and fatality of migratory bats at a wind energy facility in Alberta, Canada. Journal of Wildlife Management **75**(5): 1103-1114.

Baerwald, E. F., G. H. D'Amours, B. J. Klug and R. M. R. Barclay. 2008. Barotrauma is a significant cause of bat fatalities at wind turbines. Current Biology **18**(16): R695-R696.

Barclay, R. M. R. 1986. The echolocation calls of hoary (*Lasiurus cinereus*) and silver-haired (*Lasionycteris noctivagans*) bats as adaptations for long- versus short-range foraging strategies and the consequences for prey selection. Canadian Journal of Zoology **64**(12): 2700-2705.

Barclay, R. M. R. and L. D. Harder. 2003. Life histories of bats: life in the slow lane. Pages 209-246 in T. H. Kunz and M. B. Fenton, editors. Bat Ecology. University of Chicago Press, Chicago, Illinois.

Bennett, V. J. and A. M. Hale. 2014. Red aviation lights on wind turbines do not increase bat-turbine collisions. Animal Conservation **17**(4): 354-358.

Boyles, J. G., P. M. Cryan, G. F. McCracken and T. H. Kunz. 2011. Economic importance of bats in agriculture. Science **332**(6025): 41-42.

Brunet-Rossinni, A. K. and S. N. Austad. 2004. Ageing studies on bats: a review. Biogerontology **5**(4): 211-222.

Cleveland, C. J., M. Betke, P. Federico, J. D. Frank, T. G. Hallam, J. Horn, J. D. Lopez, G. F. McCracken, R. A. Medellin, A. Moreno-Valdez, C. G. Sansone, J. K. Westbrook and T. H. Kunz. 2006. Economic value of the pest control service provided by Brazilian free-tailed bats in south-central Texas. Frontiers in Ecology and the Environment **4**(5): 238-243.

Cryan, P. M. and R. M. R. Barclay. 2009. Causes of bat fatalities at wind turbines: hypotheses and predictions. Journal of Mammalogy **90**(6): 1330-1340.

Cryan, P. M., P. M. Gorresen, C. D. Hein, M. R. Schirmacher, R. H. Diehl, M. M. Huso, D. T. S. Hayman, P. D. Fricker, F. J. Bonaccorso, D. H. Johnson, K. Heist and D. C. Dalton. 2014. Behavior of bats at wind turbines. Proceedings of the National Academy of Sciences of the United States of America **111**(42): 15126-15131.

Falk, B., T. Williams, M. Aytekin and C. Moss. 2011. Adaptive behavior for texture discrimination by the free-flying big brown bat, *Eptesicus fuscus*. Journal of Comparative Physiology A-Neuroethology, Sensory, Neural, and Behavioral Physiology **197**(5): 491-503.

Fenton, M. B. 2013. Questions, ideas and tools: lessons from bat echolocation. Animal Behaviour **85**(5): 869-879.

Fleming, T. H. and E. R. Heithaus. 1981. Frugivorous bats, seed shadows, and the structure of tropical forests. Biotropica **13**(2): 45-53.

Frick, W. F., J. F. Pollock, A. C. Hicks, K. E. Langwig, D. S. Reynolds, G. G. Turner, C. M. Butchkoski and T. H. Kunz. 2010. An emerging disease causes regional population collapse of a common North American bat species. Science **329**(5992): 679-682.

Geipel, I., K. Jung and E. K. V. Kalko. 2013. Perception of silent and motionless prey on vegetation by echolocation in the gleaning bat *Micronycteris microtis*. Proceedings of the Royal Society B-Biological Sciences **280**(1754): 20122830.

Genzel, D., C. Geberl, T. Dera and L. Wiegrebe. 2012. Coordination of bat sonar activity and flight for the exploration of three-dimensional objects. Journal of Experimental Biology **215**: 2226-2235.

Genzel, D. and L. Wiegrebe. 2008. Time-variant spectral peak and notch detection in echolocation-call sequences in bats. Journal of Experimental Biology **211**(1): 9-14.

Goerlitz, H. R., M. Huebner and L. Wiegrebe. 2008. Comparing passive and active hearing: spectral analysis of transient sounds in bats. Journal of Experimental Biology **211:** 1850-1858.

Greif, S. and B. M. Siemers. 2010. Innate recognition of water bodies in echolocating bats. Nature Communications **1**: 107.

Griffin, D. R., F. A. Webster and C. R. Michael. 1960. The echolocation of flying insects by bats. Animal Behaviour **8**: 141-154.

Griffiths, S. R. 2013. Echolocating bats emit terminal phase buzz calls while drinking on the wing. Behavioural Processes **98**: 58-60.

Grodsky, S. M., M. J. Behr, A. Gendler, D. Drake, B. D. Dieterle, R. J. Rudd and N. L. Walrath. 2011. Investigating the causes of death for wind turbine-associated bat fatalities. Journal of Mammalogy **92**(5): 917-925.

Harvey, M. J., J. S. Altenbach and T. L. Best. 2011. Bats of the United States and Canada. Johns Hopkins University Press, Baltimore, MD.

Hayes, M. A. 2013. Bats killed in large numbers at United States wind energy facilities. Bioscience **63**(12): 975-979.

Hein, C. D., J. Gruver and E. B. Arnett. 2013. Relating pre-construction bat activity and post-construction bat fatality to predict risk at wind energy facilities: a synthesis. A report submitted to the National Renewable Energy Laboratory. Bat Conservation Inernational, Austin, TX, USA.

Horn, J. W., E. B. Arnett and T. H. Kunz. 2008. Behavioral responses of bats to operating wind turbines. Journal of Wildlife Management **72**(1): 123-132.

Hurlbert, S. H. 1984. Pseudoreplication and the design of ecological field experiments. Ecological Monographs **2**: 187-211.

Huso, M. M. P. and D. Dalthorp. 2014. A comment on bats killed in large numbers at United States wind energy facilities. Bioscience **64**(6): 546-547.

Jakobsen, L., J. M. Ratcliffe and A. Surlykke. 2013. Convergent acoustic field of view in echolocating bats. Nature **493**(7430): 93-96.

Johnson, G. D. 2005. A review of bat mortality at wind-energy developments in the United States. Bat Research News **46**(2): 45-49.

Kirk, R. E. 2010. Latin square design. Corsini Encyclopedia of Psychology, John Wiley & Sons, Inc. 1-2.

Kounitsky, P., J. Rydell, E. Amichai, A. Boonman, O. Eitan, A. J. Weiss and Y. Yovel. 2015. Bats adjust their mouth gape to zoom their biosonar field of view. Proceedings of the National Academy of Sciences of the United States of America **112**(21): 6724-6729.

Kunz, T. H., E. B. Arnett, W. P. Erickson, A. R. Hoar, G. D. Johnson, R. P. Larkin, M. D. Strickland, R. W. Thresher and M. D. Tuttle. 2007. Ecological impacts of wind energy development on bats: questions, research needs, and hypotheses. Frontiers in Ecology and the Environment **5**(6): 315-324.

Kunz, T. H., E. B. de Torrez, D. Bauer, T. Lobova and T. H. Fleming. 2011. Ecosystem services provided by bats. Annals of the New York Academy of Sciences **1223:** 1-38.

Langwig, K. E., W. F. Frick, J. T. Bried, A. C. Hicks, T. H. Kunz and A. M. Kilpatrick. 2012. Sociality, density-dependence and microclimates determine the persistence of populations suffering from a novel fungal disease, white-nose syndrome. Ecology Letters **15**(9): 1050-1057.

Ledec, G. C., K. W. Rapp and R. G. Aiello. 2011. Greening the Wind: Environmental and Social Considerations for Wind Power Development in Latin America and Beyond. Energy Unit, Sustainable Development Department, Latin America and Caribbean Region, The World Bank. Washington, D. C., 170 pp.

Long, C. V., J. A. Flint and P. A. Lepper. 2011. Insect attraction to wind turbines: does colour play a role? European Journal of Wildlife Research **57**(2): 323-331.

Mackey, R. L. and R. M. R. Barclay. 1989. The influence of physical clutter and noise on the activity of bats over water. Canadian Journal of Zoology **67**(5): 1167-1170.

McAlexander, A. 2013. Evidence that bats perceive wind turbine surfaces to be water. Thesis, Texas Christian University.

Melcón, M. L., H.-U. Schnitzler and A. Denzinger. 2009. Variability of the approach phase of landing echolocating greater mouse-eared bats. Journal of Comparative Physiology A-Neuroethology, Sensory, Neural, and Behavioral Physiology **195**(1): 69-77.

Mello, M. A. R., F. M. D. Marquitti, P. R. Guimaraes, E. K. V. Kalko, P. Jordano and M. A. M. de Aguiar. 2011. The missing part of seed dispersal networks: structure and robustness of bat-fruit interactions. PLOS ONE **6**(2).

Mogensen, F. and B. Møhl. 1979. Sound radiation patterns in the frequency domain of cries from a Vespertilionid bat. Journal of Comparative Physiology A-Neuroethology, Sensory, Neural, and Behavioral Physiology **134**: 165-171.

Mora, E. C., S. Macias, J. Hechavarría, M. Vater and M. Kössl. 2013. Evolution of the heteroharmonic strategy for target-range computation in the echolocation of Mormoopidae. Frontiers in Physiology **4**: 141.

Moss, C. F., C. Chiu and A. Surlykke. 2011. Adaptive vocal behavior drives perception by echolocation in bats. Current Opinion in Neurobiology **21**(4): 645-652.

Moss, C. F. and A. Surlykke. 2001. Auditory scene analysis by echolocation in bats. Journal of the Acoustical Society of America **110**(4): 2207-2226.

O'Shea, T. J., M. A. Bogan and L. E. Ellison. 2003. Monitoring trends in bat populations of the United States and territories: status of the science and recommendations for the future. Wildlife Society Bulletin **31**(1): 16-29.

Obrist, M. K. and J. J. Wenstrup. 1998. Hearing and hunting in red bats (*Lasiurus borealis*, Vespertilionidae): audiogram and ear properties. Journal of Experimental Biology **201**(1): 143-154.

Pierce, A. D. 1989. Acoustics: An Introduction to its Physical Principles and Applications. Acoustical Society of America, Woodbury, NY.

Podlutsky, A. J., A. M. Khritankov, N. D. Ovodov and S. N. Austad. 2005. A new field record for bat longevity. Journal of Gerontology Series A-Biological Sciences and Medical Sciences **60**(11): 1366-1368.

Ratcliffe, J. M., C. P. Elemans, L. Jakobsen and A. Surlykke. 2013. How the bat got its buzz. Biology Letters **9**(2): 1-4.

REN21. 2015. Renewables 2015 Global Status Report. Paris: REN21 Secretariat.

Rollins, K. E., D. K. Meyerholz, G. D. Johnson, A. P. Capparella and S. S. Loew. 2012. A forensic investigation into the etiology of bat mortality at a wind farm: barotrauma or traumatic injury? Veterinary Pathology **49**(2): 362-371.

Rydell, J., L. A. Miller and M. E. Jensen. 1999. Echolocation constraints of Daubenton's bat foraging over water. Functional Ecology **13**: 247-255.

Schmieder, D. A., T. Kingston, R. Hashim, and B. M. Siemers. 2012. Sensory constraints on prey detection performance in an ensemble of vespertilionid understorey rain forest bats. Functional Ecology **26**: 1043-1053.

Siemers, B. M., W.-P. Stilz and H.-U. Schnitzler. 2001. The acoustic advantage of hunting at low heights above water: behavioural experiments on the European "trawling" bats *Myotis capaccinii*, *M. dasycneme* and *M. daubentonii*. Journal of Experimental Biology **204**: 3843-3854.

Simmons, J. A., M. J. Ferragamo and C. F. Moss. 1998. Echo-delay resolution in sonar images of the big brown bat, *Eptesicus fuscus*. Proceedings of the National Academy of Sciences of the United States of America **95**: 12647-12652.

Simmons, J. A., E. G. Freedman, S. B. Stevenson, L. Chen and T. J. Wohlgenant. 1989. Clutter interference and the integration time of echoes in the echolocating bat, *Eptesicus fuscus*. Journal of the Acoustical Society of America **86**(4): 1318-1382.

Simmons, J. A., W. A. Lavender, B. A. Lavender, J. E. Childs, K. Hulebak, M. R. Rigden, J. Sherman, B. Woolman and M. J. O'Farrell. 1978. Echolocation by free-tailed bats (*Tadarida*). Journal of Comparative Physiology **125**(4): 291-299.

Stilz, W.-P. and H.-U. Schnitzler. 2012. Estimation of the acoustic range of bat echolocation for extended targets. Journal of the Acoustical Society of America **132**(3): 1765-1775.

Surlykke, A. and C. F. Moss. 2000. Echolocation behavior of big brown bats, *Eptesicus fuscus*, in the field and the laboratory. Journal of the Acoustical Society of America **108**(5): 2419-2429.

von Frenckell, B. and R. M. R. Barclay. 1987. Bat activity over calm and turbulent water. Canadian Journal of Zoology **65**: 219-222.

Vorländer, M. and E. Mommertz. 2000. Definition and measurement of random-incidence scattering coefficients. Applied Acoustics **60**: 187-199.

Winfree, R., I. Bartomeus and D. P. Cariveau. 2011. Native pollinators in anthropogenic habitats. Annual Review of Ecology, Evolution, and Systematics **42:** 1-22.

VITA

Personal Background

Brad Rhett Yuen
Kaneohe, Hawaii
Son of Kirk & Kathy Yuen

Education

2005 Diploma, Theodore Roosevelt High School, Honolulu, HI
2009 Bachelor of Arts, Ecology and Conservation Biology, Boston University, Boston, MA
2015 Master of Science, Environmental Science, Texas Christian University, TX

Experience

2014-Present Teaching Assistantship, Texas Christian University
2013 Field Technician, Texas Christian University
2012 Biological Field Technician, University of Nebraska-Lincoln
2011 Research Assistant, Instituto de Ecología, A.C.
2009-2010 AmeriCorps-KUPU Intern, U.S. Geological Survey at Kilauea Field Station
2009 Biological Science Technician, U.S. Geological Survey at Kilauea Field Station
2008-2009 Lab Assistant, Department of Biology, Boston University
2008 Field Research Assistant, Boston University

Presentations

Yuen, B. 2015. Bats: their role in the environment and the value of the ecosystem services they provide. Lecture, Contemporary Issues in Environmental Science, Texas Christian University. Fort Worth, TX.

Yuen, B., V. Bennett, A. Hale, B. Cooper. 2015. Surface texture discrimination using synthetic bat echolocation calls: implications for reducing bat fatalities at wind turbines. Michael and Sally McCracken Student Research Symposium. Texas Christian University. Fort Worth, TX.

Yuen, B., P. M. Gorresen, C. Pinzari, F. Bonaccorso. 2010. Feeding activity as a measure of habitat quality for the Hawaiian hoary bat. 18th Annual Hawaii Conservation Conference. Honolulu, HI.

Awards

2015 Best graduate teaching assistant
2015 1st place graduate student poster, Texas Christian University

ABSTRACT

SURFACE TEXTURE DIFFERENTIATION USING SYNTHETIC BAT ECHOLOCATION CALLS: IMPLICATIONS FOR REDUCING BAT FATALITIES AT WIND TURBINES

by Brad Rhett Yuen, M.S., 2015
School of Geology, Energy, and the Environment
Texas Christian University

Thesis Advisor: Dr. Victoria J. Bennett, Assistant Professor of Environmental Science

Committee Members: Dr. Amanda M. Hale, Associate Professor of Biology

Dr. Brenton G. Cooper, Associate Professor of Psychology

Large numbers of bats are killed annually at wind energy facilities. The patterns of these fatalities suggest attraction to wind turbines. One reason bats may be attracted to wind turbines is that they misperceive the smooth, painted surfaces of wind turbine towers to be water. In 2014, we conducted an ultrasonic playback experiment using synthetic bat echolocation calls to determine if texturing wind turbine paint could reduce the acoustic similarity between wind turbine tower surfaces and water. Our playback experiment revealed measurable intensity, spectral, and temporal differences between ultrasonic echoes reflecting off of smooth and textured surfaces. These differences were most pronounced at shallower angles of incidence, at higher call frequencies, and for textures with larger particle sizes. If water misperception is contributing to bat fatalities at wind turbines, then our results tentatively suggest that texturing wind turbine towers with coarse textures (1.4 – 2.0 mm) could be a mitigating strategy.